

SPECTRAL EVOLUTION OF THE EXTRAORDINARY TYPE II_n SUPERNOVA 2006gy

NATHAN SMITH^{1,2}, RYAN CHORNOCK¹, JEFFREY M. SILVERMAN¹, ALEXEI V. FILIPPENKO¹, & RYAN J. FOLEY^{1,3,4}

Draft version October 22, 2018

ABSTRACT

We present a detailed analysis of the extremely luminous and long-lasting Type II_n supernova (SN) 2006gy using spectra obtained between days 36 and 237 after explosion. We derive the temporal evolution of the effective temperature, radius, blast-wave and SN-ejecta expansion speeds, and bolometric luminosity, as well as the progenitor wind density and total swept-up mass overtaken by the shock. SN 2006gy can be interpreted in the context of shock interaction with a dense circumstellar medium (CSM), but with quite extreme values for the CSM mass of $\sim 20 M_{\odot}$ and a SN explosion kinetic energy of at least 5×10^{51} erg. A key difference between SN 2006gy and other SNe II_n is that, owing to its large amount of swept-up mass, the interaction region remained opaque much longer. At early times, H α emission-line widths suggest that the photosphere is ahead of the shock, and photons diffuse out through the opaque CSM shell. The pivotal transition to optically thin emission begins to occur around day 110, when we start to see a decrease in the blackbody radius R_{BB} and strengthening tracers of the post-shock shell. (A lingering puzzle, however, is that the late-time data require additional energy not traced by CSM-interaction diagnostics.) From the evolution of pre-shock velocities, we deduce that the CSM was ejected by the progenitor star in a $\sim 10^{49}$ erg precursor event ~ 8 yr before the explosion. The large CSM mass definitively rules out models involving stars with initial masses of $\lesssim 10 M_{\odot}$. If the pre-SN mass budget also includes the likely SN ejecta mass of 10–20 M_{\odot} and the distant $> 10 M_{\odot}$ shell inferred elsewhere for the infrared light echo, then even massive $M_{\text{ZAMS}}=30\text{--}40 M_{\odot}$ progenitor stars are inadequate. At roughly solar metallicity, substantial mass loss probably occurred during the star's life, so SN 2006gy's progenitor is more consistent with sequential giant luminous blue variable eruptions or pulsational pair-instability ejections in extremely massive stars with initial masses above 100 M_{\odot} . This requires significant revision to current paradigms of massive-star evolution.

Subject headings: circumstellar matter — stars: evolution — supernovae: individual (SN 2006gy)

1. INTRODUCTION

The subclass of Type II_n supernovae (SNe II_n) provides a unique probe of extreme pre-SN mass loss in massive stars. The II_n designation (Schlegel 1990; Filippenko 1997) refers to either (1) very narrow (widths of tens to a few hundred km s^{-1}) H emission lines that are thought to arise from photoionized pre-shock circumstellar gas (e.g., Salamanca et al. 1998, 2002; Chugai et al. 2002), or (2) intermediate-width (typically $(1\text{--}5) \times 10^3 \text{ km s}^{-1}$) H lines from post-shock gas accelerated as the SN ejecta collide with the circumstellar medium (CSM), sometimes with extended wings broadened by electron scattering (Chugai & Danziger 1994; Chugai 2001; Chugai et al. 2004; Dessart et al. 2009).

SNe II_n show a huge range in bolometric luminosity and spectral properties, presumably resulting from a wide range of pre-SN CSM environments and intrinsic SN properties. Their visual-wavelength luminosity in excess of a normal Type II-plateau (II-P) SN is powered largely by reprocessing SN ejecta kinetic energy through shocks arising from CSM interaction (Chugai 1990; Chevalier 1977, 2003). Depending on the strength of CSM interaction and optical depth of the emitting region, SNe II_n can potentially be luminous X-ray and radio emitters

for years after explosion, as in the cases of SNe 1988Z, 1986J, 1980K, 1978K, and others (e.g., Canizares et al. 1982; Leibundgut et al. 1991; Ryder et al. 1992; Bregman & Pildis 1992; Van Dyk et al. 1993; Williams et al. 2002; Pooley et al. 2002; Schlegel & Petre 2006).

At the time of discovery, SN 2006gy was by far the most luminous known SN II_n. It exploded in the peculiar S0/Sa galaxy NGC 1260 (Figure 1), and the early data and significance of this SN were first discussed by Ofek et al. (2007) and Smith et al. (2007; Paper I hereafter). SN 2006gy was extraordinary in that it had a peak luminosity more than 100 times higher than that of a normal SN II-P, it had a remarkably slow rise time of ~ 70 days, the light-curve shape was unusually rounded for a SN II_n (Paper I), and the CSM environment was extremely dense and extended. Analysis of the light-curve rise time, including pre-discovery photometry, implied a rough explosion date of 2006 Aug. 20 (Paper I; UT dates are used throughout this paper), which we shall adopt here. SN 2006gy was located only $1''$ (~ 300 pc) from the active nucleus of NGC 1260, which has provided enduring difficulty in studying the object as it fades, and the SN appeared to be located along a dust lane with superposed emission from H II regions (Ofek et al. 2007; Paper I; Smith et al. 2008b; Figure 1). NGC 1260's star-formation rate of $\sim 1.2 M_{\odot} \text{ yr}^{-1}$ indicated by its infrared (IR) emission makes it plausible that the progenitor of SN 2006gy was a massive star associated with a young stellar population (Ofek et al. 2007; Paper I). The host

¹ Department of Astronomy, University of California, Berkeley, CA 94720-3411.

² Email: nathans@astro.berkeley.edu.

³ Center for Astrophysics, 60 Garden St., Cambridge, MA 02138.

⁴ Clay Fellow.

galaxy’s average metallicity is 0.6–0.7 Z_{\odot} , and SN 2006gy occurred near the nucleus, so its environment was *not* low metallicity. This influences its pre-SN mass loss and any models for the progenitor star’s evolution.

The high luminosity and large total radiated energy of SN 2006gy – exceeding 10^{51} erg in visual light alone – raised new questions about the engine that powers the luminosity, which we have discussed in detail in Paper I. In brief, the two leading candidates are CSM interaction, motivated by the Type II_n spectrum, or radioactive decay from several M_{\odot} of ^{56}Ni generated in a pair-instability supernova (PISN). Neither hypothesis matches straightforward expectations. The CSM interaction hypothesis is complicated by the astonishingly large required mass (10–20 M_{\odot}) in the CSM environment, which in turn seems to require an explosive or impulsive shell ejection to occur within a few years immediately preceding the SN (see Paper I; Smith & McCray 2007; Woosley et al. 2007). Key shock diagnostics such as $\text{H}\alpha$ and X-ray emission in SN 2006gy, however, are far weaker than naive expectations for CSM interaction.

On the other hand, the PISN hypothesis is complicated by the fact that true PISNe (Barkat et al. 1967; Rakavy & Shaviv 1967; Bond et al. 1984; Heger & Woosley 2002) are only expected for extremely massive progenitor stars at low metallicity where mass loss is thought to be unimportant (e.g., Heger et al. 2003), and the lethargic light-curve evolution of SN 2006gy was not slow enough to match predictions for PISNe (Scannapieco et al. 2005). Effects of close binary evolution, such as common-envelope ejection or mergers, have also been discussed (Ofek et al. 2007; Portegies Zwart & van den Heuvel 2007), although these do not address the physical origin of the high luminosity itself. Agnoletto et al. (2009) invoked a combination of these extraordinary conditions, placing somewhat less extreme demands than for any single mechanism alone: radioactive decay from 1–3 M_{\odot} of ^{56}Ni plus extraordinarily strong CSM interaction with a 6–10 M_{\odot} pre-SN envelope. In any case, SN 2006gy stretched the limits for plausible physical explanations of its energy source.

While the PISN hypothesis has been difficult to disprove, there is a potential way to reconcile the CSM interaction model with the apparent difficulties posed by observations. Smith & McCray (2007) proposed that with the high optical depths that might occur when a blast wave overtakes an opaque pre-SN shell, radiative diffusion may be important, so that X-ray and $\text{H}\alpha$ emission would be weak compared to other SNe II_n. In this model, the weak $\text{H}\alpha$ and unabsorbed soft X-rays occur after the blast wave exits the opaque shell and encounters additional CSM downstream, while radiation continues to diffuse out from shock-deposited thermal energy in the slowly expanding opaque shell. Woosley et al. (2007) considered a similar idea, but proposed that the pre-SN ejection in question was triggered by the pulsational pair instability. This occurs as a result of the same pair instability that leads to a PISN, but the explosion is insufficient to fully unbind the star, resulting in a lower-energy ejection of only the outer envelope instead (Heger & Woosley 2002; Heger et al. 2003). In their model, this occurred in the late nuclear burning phases of a star with an initial mass of 110 M_{\odot} and with lower mass-loss rates than have traditionally been adopted in stellar evolution

calculations for stars at solar metallicity.

The idea that a very massive star retains a massive H envelope until core collapse, while experiencing eruptive mass ejection analogous to giant eruptions of luminous blue variables (LBVs) like η Carinae, has interesting implications for understanding massive-star evolution, as discussed elsewhere (see Paper I; Smith & Owocki 2006; Gal-Yam et al. 2007). Although it defies current paradigms of stellar evolution theory, the LBV/SN II_n connection has recently been reinforced by the direct detection of a progenitor of the Type II_n SN 2005gl, which resembled a very luminous LBV (Gal-Yam & Leonard 2009). Nevertheless, the true nature of the progenitor of SN 2006gy remains uncertain.

It was hoped that late-time observations could settle these mysteries about the power source for the tremendous luminosity of SN 2006gy. Smith et al. (2008b) reported optical and near-IR photometry and spectroscopy obtained after one year. The SN was below detection limits at visual wavelengths, but in the near-IR it was still at least as luminous as the peak of a normal SN II-P. The late-time spectrum revealed no clear detection of features associated with SN 2006gy, although the object is only 1'' from the bright nucleus as noted above. However, these spectra yielded upper limits to any late-time post-shock $\text{H}\alpha$ emission of $\lesssim 10^{39}$ erg s⁻¹, which is a factor of ~ 400 lower than for a less luminous SN II_n such as SN 1988Z (e.g., Aretxaga et al. 1999) at a comparable epoch. (The luminous SN II_n 2006tf, by contrast, showed strong and easily detected broad $\text{H}\alpha$ at late times; Smith et al. 2008a.) If CSM interaction were an important engine at late times, one would also expect strong X-ray emission or radio emission, which was not the case (Bietenholz & Bartel 2007; Smith et al. 2008b). Therefore, Smith et al. (2008b) ruled out continuing CSM interaction as the late-time luminosity source, and proposed either radioactive decay obscured by dust or, more likely, an IR echo from a distant dust shell.

Subsequently, Agnoletto et al. (2009) and Kawabata et al. (2009) also presented late-time optical and IR photometry of SN 2006gy, including detections and limits consistent with Smith et al. (2008b). Kawabata et al. claimed a detection of late-time (>1 yr) spectral features associated with SN 2006gy, although some of the lines are questionable given their peculiar or unknown identifications. Their estimate of the late-time $\text{H}\alpha$ flux of $\sim 10^{39}$ erg s⁻¹ agrees with the upper limits of Smith et al. (2008b), confirming that the late-time luminosity cannot be powered by CSM interaction. Kawabata et al. proposed that their late-time photometric detection was consistent with a radioactive decay tail from 15 M_{\odot} of ^{56}Ni (Nomoto et al. 2007) if γ -rays from the decay are not fully trapped. A light echo from a massive CSM shell ejected ~ 1500 yr before core collapse, as proposed by Smith et al. (2008b), is the favored interpretation for the late-time IR luminosity in view of more recent evidence, however. In a companion paper, we discuss the IR-echo hypothesis in more detail (Miller et al. 2009b).

Although SN 2006gy had the highest peak luminosity of any known SN when it was discovered (Ofek et al. 2007; Smith et al. 2007), subsequent discoveries of SN 2005ap⁵

⁵ Although the explosion of SN 2005ap obviously occurred before SN 2006gy, its distance and high luminosity were recognized later

TABLE 1
SPECTROSCOPIC OBSERVATIONS OF SN 2006GY

UT Date	Day ^a	Instrument	Range ^b (Å)	$\lambda/\Delta\lambda$	$T_{\text{BB}}(\text{cont.})^c$ (10^3 K)	EW(H α) (Å)	$F(\text{H}\alpha)$ ($\text{erg s}^{-1} \text{cm}^{-2}$)	H α /H β^d
2006 Sep. 25	36	Kast/Lick	3500–9600	700	12.0(3.0)	−56.1(3)	$13.5(0.8)\times 10^{-14}$	2.9(0.2)
2006 Oct. 24	65	Kast/Lick	3500–9600	700	12.0(0.8)	−28.0(2)	$10.4(0.6)\times 10^{-14}$	2.9(0.3)
2006 Oct. 30	71	Kast/Lick	3500–9600	700	11.0(0.7)	−23.5(2)	$8.7(0.5)\times 10^{-14}$	3.2(0.3)
2006 Nov. 20	92	Kast/Lick	5450–6800	1000	8.5(0.9)	−18.0(2)	$5.4(0.4)\times 10^{-14}$...
2006 Nov. 21	93	LRIS/Keck	3500–9100	1000	9.00(0.3)	−22.0(1)	$6.9(0.3)\times 10^{-14}$	6.8(2)
2006 Nov. 24	96	DEIMOS/Keck	4500–7100	8000	8.80(0.4)	−27.7(1)	$7.8(0.2)\times 10^{-14}$	6.5(2)
2006 Dec. 20	122	Kast/Lick	3500–9600	700	7.10(0.3)	−57.4(4)	$10.0(0.4)\times 10^{-14}$	≥ 50
2006 Dec. 23	125	DEIMOS/Keck	4500–7100	8000	7.05(0.4)	−61.4(1)	$10.1(0.2)\times 10^{-14}$	45(15)
2006 Dec. 25	127	LRIS-P/Keck	3500–9050	1000	7.05(0.3)	−64.8(2)	$10.5(0.4)\times 10^{-14}$	65(20)
2007 Jan. 13	145	LRIS/Keck	3500–9050	1000	6.9(0.8)	−104(4)	$11.9(0.4)\times 10^{-14}$	128(40)
2007 Jan. 21	153	LRIS-P/Keck	3500–9050	1000	6.60(0.3)	−133(5)	$9.17(0.3)\times 10^{-14}$	105(30)
2007 Jan. 22	154	DEIMOS/Keck	4500–7100	8000	6.2(0.9)	−114(2)	$9.14(0.2)\times 10^{-14}$	110(30)
2007 Jan. 26	158	Kast/Lick	4200–9600	700	6.50(0.4)	−108(6)	$8.1(0.4)\times 10^{-14}$	(abs.)
2007 Feb. 14	177	LRIS-P/Keck	3500–9050	1000	6.55(0.3)	−103(4)	$5.15(0.4)\times 10^{-14}$	100(30)
2007 Feb. 16	179	DEIMOS/Keck	4500–7100	8000	6.45(0.7)	−115(3)	$5.62(0.2)\times 10^{-14}$	92(20)
2007 Mar. 18	209	LRIS-P/Keck	3500–9050	1000	6.45(0.3)	−67.9(4)	$2.4(0.2)\times 10^{-14}$	78(15)
2007 Apr. 15	237	LRIS-P/Keck	3500–9050	1000	5.90(0.3)	−33.5(4)	$1.1(0.2)\times 10^{-14}$...
2007 Oct. 16	421	LRIS-P/Keck	3500–9050	1000

^a Days since 2006 Aug. 20, the presumed time of explosion adopted from Paper I. This is ~ 29 days before discovery.

^b Spectral range in rest wavelength.

^c Approximate blackbody temperature indicated by the continuum shape in dereddened visual-wavelength spectra (see Fig. 4). Here and elsewhere, uncertainties are given in parentheses. The temperature derived from the continuum shape for day 36 is less certain for reasons described in the text.

^d The H α /H β emission flux ratio measured after the spectra are dereddened. Many of these values are highly uncertain because at later times H β emission is weak, is blended with Fe II lines, and is affected by deep absorption.

(Quimby et al. 2007) and SN 2008es (Gezari et al. 2009; Miller et al. 2009a) have raised the bar, with peak luminosities almost a factor of 2 higher. For all three events, the integrated radiated energy in the first few months was of order 10^{51} erg, and $\sim 2\times 10^{51}$ erg in the case of SN 2006gy. These objects therefore present a new and fundamental challenge to SN physics. With a peak luminosity ~ 1 mag fainter than that of SN 2006gy, the Type IIn SN 2006tf seems to mark the upper bound of what can be achieved with standard CSM interaction because of optical-depth limitations (see Smith et al. 2008a). Standard CSM interaction, taken here to mean that the observed luminosity arises from direct cooling by the radiative post-shock gas, therefore has difficulty accounting for the higher luminosities of SNe 2006gy, 2005ap, and 2008es. This leads one to suspect that high optical depths and consequent delayed effects of radiative diffusion play an essential role (Smith & McCray 2007).

We have the opportunity to focus in detail on SN 2006gy because it was closer ($d = 73.1$ Mpc) than either SN 2005ap ($d \approx 1200$ Mpc) or SN 2008es (~ 900 Mpc), so available spectra of SN 2006gy are of higher quality. A consistent theme throughout this paper will be that although there are clear signs of CSM interaction in the spectrum, the level of CSM interaction one infers from spectral diagnostics seems vastly insufficient to power the visual-wavelength continuum luminosity of SN 2006gy. This amplifies comments we made in Paper I regarding its relatively weak H α and X-ray emission. The insufficient level of CSM interaction in SN 2006gy is particularly relevant to SN 2005ap and SN 2008es, since both of those events appeared to be Type II-linear (II-L) events, lacking any narrow H α emission indicative of the

(Quimby et al. 2007).

CSM interaction that one sees in SNe IIn. All other top contenders with peak M_R brighter than -20 mag were of Type IIn.

In Paper I, we considered basic implications of the energy budget of SN 2006gy, while Smith & McCray (2007) and Smith et al. (2008b) have discussed additional aspects of the evolving light curve and late-time photometry. Independent observations of SN 2006gy have been discussed by Ofek et al. (2007), Kawabata et al. (2009), and Agnoletto et al. (2009). In this paper we undertake a more detailed analysis of our multi-epoch spectra, concentrating on the main light-curve peak when SN 2006gy released most of its radiated energy. We adopt many of the same basic properties as in Paper I: $d = 73.1$ Mpc, $z = 0.0179$, and $A_R = 1.68$ mag. We present the spectral observations in §2 (including additional spectra not published in Paper I), and we examine the main results of these spectra in §3. In §4 we synthesize the observations into a general scenario to explain the SN, and we also discuss implications for SNe and massive-star evolution.

2. OBSERVATIONS

2.1. Lick and Keck Spectroscopy

We obtained visual-wavelength spectra of SN 2006gy at several times during the first year after explosion, as well as at one epoch more than 1 yr after discovery. Table 1 summarizes the observational parameters for each epoch. These were obtained at the Keck Observatory using the low-resolution imaging spectrometer (LRIS; Oke et al. 1995) and the Deep Imaging Multi-Object Spectrograph (DEIMOS; Faber et al. 2003). We also obtained spectra using the Kast double spectrograph (Miller & Stone 1993) mounted on the Lick Observatory 3-m Shane telescope. The spectra at early times were all obtained with the long slit oriented at the parallactic angle (Filippenko

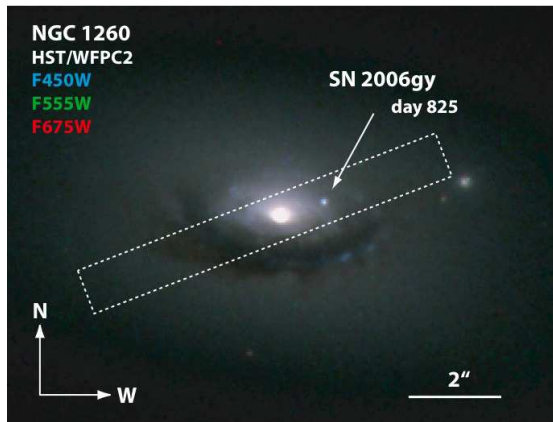


FIG. 1.— Color *HST*/WFPC2 image of NGC 1260 and SN 2006gy obtained ~ 2 yr after explosion (on day 825), with the F450W filter in blue, F555W in green, and F675W in red. (The acquisition, reduction, and analysis of these late-time *HST*/WFPC2 data are presented in a companion paper; Miller et al. 2009b.) At early epochs when the SN dominated the light, the spectroscopic slit aperture was oriented at the parallactic angle, while at later epochs the slit was oriented at a position angle of $285^\circ - 291^\circ$ such that it passed through the SN and the galactic nucleus so that we could be sure of the supernova’s position. A typical slit aperture is shown.

1982) to minimize losses caused by atmospheric dispersion, while later spectra when the SN faded were oriented with the slit passing through the nucleus of NGC 1260 (see Figure 1).

The spectra were reduced using standard techniques (e.g., Foley et al. 2003). Our spectra on days 36, 71, and 96 were already presented in Paper I, and additional details of the data-reduction steps can be found there. The spectra were corrected for atmospheric extinction (Bessell 1999; Matheson et al. 2000) using standard stars observed at an airmass similar to that of the SN and then flux calibrated using our photometry of SN 2006gy. When correcting the spectra for extinction, we adopt a host-galaxy extinction of $A_R = 1.25 \pm 0.25$ mag ($A_V = 1.67$ mag; $E(B-V) = 0.54$ mag) for SN 2006gy in addition to the Galactic extinction of $A_R = 0.43$ mag ($A_V = 0.57$ mag; $E(B-V) = 0.18$ mag), and we use $R = 3.1$ and the reddening curve of Cardelli et al. (1989), as described in Paper I. As noted there, the Na I D absorption in the spectrum of SN 2006gy may suggest even higher reddening than we have assumed here, so our luminosity estimates for SN 2006gy are conservative. The observed and flux-calibrated spectra of SN 2006gy are shown in Figure 2. In all of the spectra presented here, the observed wavelengths have been corrected to the rest-frame wavelengths using redshift $z = 0.0179$ (see Paper I).

2.2. Difficulties Posed by the Environment

Photometric and spectroscopic observations of SN 2006gy are challenging because the SN is located only $\sim 1''$ from the bright galactic nucleus of NGC 1260 (Figure 1). This is especially true at late times when the SN has faded; during the main light-curve peak, SN 2006gy was much stronger than shown in Figure 1, dominating the surrounding flux (see Fig. 1 in Paper I). There is a steep intensity gradient in the underlying galaxy light that includes a dust lane and velocity-dependent emission lines from H II regions that follow the rotation curve of the galaxy (Figure 1; Paper I; Ofek et al. 2007; Smith et al. 2008b). To subtract host-galaxy

light, we sampled emission along the slit immediately on either side of SN 2006gy (an example slit is shown in Figure 1). We checked carefully to make sure that the sky-subtraction procedure did not artificially introduce false narrow absorption components in this procedure. We determined that such oversubtraction did not affect the data; H, He I, and other lines show similar narrow blueshifted absorption profiles, even though only H α and [N II] are strong in the background, and the observed narrow absorption components weaken systematically with time as the SN fades.

To check the uncertainty introduced by the difficult host-galaxy subtraction on such a strong intensity gradient near the nucleus, we compare (Figure 3) two relatively late-time spectra of SN 2006gy on days 177 and 209 to an extracted spectrum of the background galaxy at the same position. This background spectrum is from day 421 when the SN is no longer detected in our data. The flat continuum level here has been scaled to the background intensity of $\sim 2 \times 10^{-16}$ erg s $^{-1}$ cm $^{-2}$ \AA^{-1} arcsec 2 measured in the WFPC2 image. At the shortest wavelengths, the background flux that would contaminate a $\sim 1''$ point source is comparable to the SN flux at late times, so careful subtraction is important. Indeed, below $\lambda \approx 4500$ \AA , late-time spectra of the SN are nearly identical to the background, so we have some concern that even our background-subtracted spectra may still include substantial galaxy light in the blue.

In order to evaluate the level of remaining host-galaxy contamination even after this baseline subtraction (which may be imperfect because of differing slit-width/seeing combinations), we experimented with subtracting additional galaxy light using the day 421 spectrum to represent the background at the SN position. The day 421 spectrum shows strong, narrow H α and [N II] emission lines from H II regions. The most additional galaxy light one can subtract is the amount which causes the nebular [N II] line to disappear in the SN spectrum; subtracting more than this would cause a spurious absorption feature at 6583 \AA . Using this criterion, the days 177 and 209 spectra with the most possible host-galaxy light subtracted are shown in Figure 3 with gray tracings (*orange in the online edition*). The resulting spectra have weaker flux and steeper continua at the shortest wavelengths. Longward of 5000 \AA , the contrast of some spectral features is stronger but the spectra are otherwise very similar. We suspect, however, that this may be an oversubtraction, because the method assumes that the SN has no intrinsic nebular emission from H α and [N II], whereas earlier spectra show variable intrinsic fluxes of these narrow lines, and the day 179 DEIMOS spectrum with high resolution shows a resolved narrow H α line profile consistent with earlier spectra when the line was stronger.

Therefore, throughout this paper we adopt the original method, used consistently for all observed epochs, of subtracting the background by sampling emission along the slit on either side of the SN. The potentially oversubtracted spectra in Figure 3 are useful, however, to remind us of the level of uncertainty introduced by possible remaining galaxy light in the data. The differences introduced by the additional subtraction are not severe – they are comparable, for example, to the differences between LRIS and DEIMOS spectra at a given epoch (see Fig-

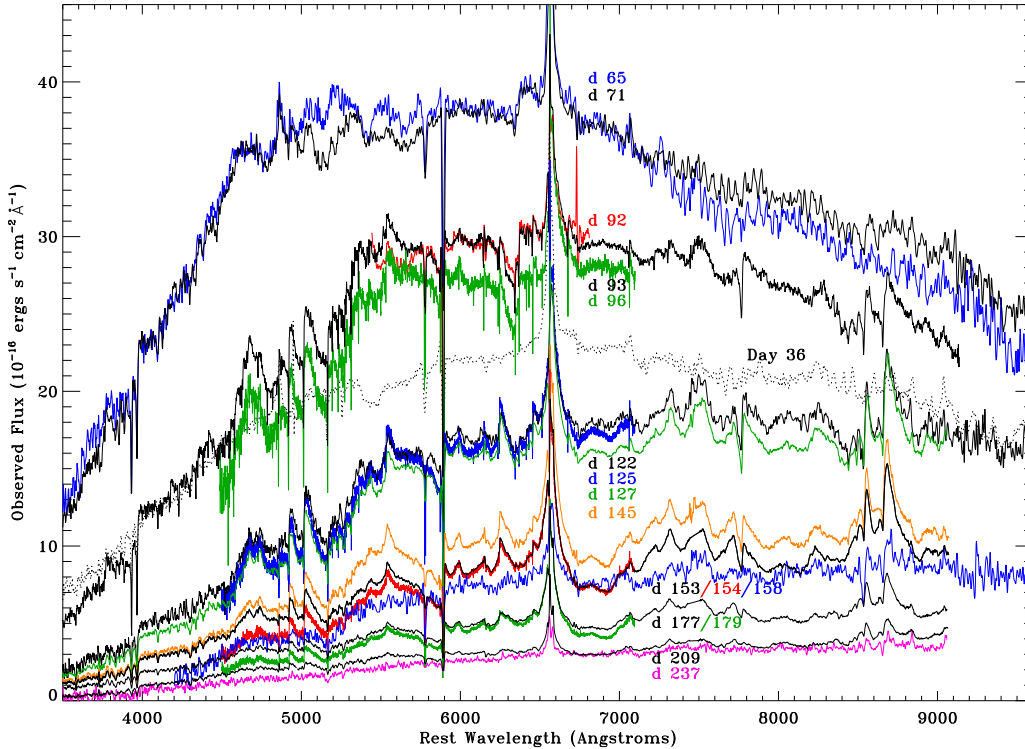


FIG. 2.— Observed spectra of SN 2006gy during the main light-curve peak on the days indicated (see Table 1), plotted on a linear intensity scale. These have not been corrected for any extinction. The dashed line is the day 36 spectrum, while the SN was still rising.

ure 4). If this contamination were as severe as the worst case represented in Figure 3, then the way that the additional subtraction of host-galaxy light would alter our analysis is that at late times after day 150 (and *only* at late times), we would derive a continuum temperature (§3.2) that is ~ 5 –10% lower and an $H\alpha$ equivalent width (§3.4.1) that is a few percent larger. Such differences are consistent with our estimated uncertainties, so it would not significantly affect our analysis. The subtraction issues discussed here would not alter the measurements of line flux and luminosity, and our conclusions do not rely on the flux at the shortest wavelengths.

The inset of Figure 3 shows in detail the spectral region near $H\alpha$. In our late-time spectrum on day 421, we see no evidence for broad post-shock $H\alpha$ emission that might arise from late-time CSM interaction, as we reported earlier (Smith et al. 2008b). The continuum underlying the narrow $H\alpha$ and $[N\ II]$ emission lines is flat, in stark contrast to earlier epochs when broad $H\alpha$ was present. Kawabata et al. (2009) reported broad $H\alpha$ emission on day 394, estimated from a raised flux level in the gap between $H\alpha$ and $[N\ II]\ \lambda 6583$. Figure 3 shows that at higher spectral resolution, this feature is not seen in our data on day 421. It therefore seems possible that the excess flux reported by Kawabata et al. (2009) may have been a blend of the wings of narrow $H\alpha$ and $[N\ II]$ emission lines in their lower-resolution spectra, and may not have been attributable to the SN.

In general, our flux-calibrated spectra give reliable and self-consistent results. Compare, for example, the pair of spectra in Figures 2 and 4 on days 93 and 96, or the pair on days 122 and 125. These were obtained only a few days apart with different instruments on different telescopes, but the flux calibration, continuum slopes, and

relative line strengths agree remarkably well except perhaps for the strengths of some of the narrowest emission or absorption features that are affected by the different instrument spectral resolutions.

We did encounter a potential problem in calibrating our spectra, however, and that was for the 2006 Sep. 25 (day 36) spectrum obtained at Lick Observatory. This was our first spectrum of SN 2006gy, calibrated with standard stars that differed from those of all other epochs; more importantly, the blue-channel flatfield lamp on the Kast spectrograph was not working on this night, so we had to use a flatfield observation from a different observing run. These issues compromise the reliability of the flux calibration and continuum slope on day 36, which is important for the resulting continuum temperature that is derived on this epoch. The red channel should not have been affected by the problematic blue-channel flatfield lamp, and this set of problems did not affect the remaining epochs of spectra. We therefore regard the blue continuum shape on day 36 with caution when deriving physical quantities in our analysis. On the other hand, the strange continuum shape may be real and caused by unusual physical circumstances; it could result from higher extinction due to time-dependent circumstellar reddening, for example, since at that early time the optical depth was very high, as we discuss below. The dereddened spectra for all epochs are shown in Figure 4. We adopted a correction of $E(B - V) = 0.723$ mag (see Paper I), although for day 36 we also show an additional reddening correction of $E(B - V) = 1.0$ mag.

3. RESULTS

3.1. Overall Spectral Morphology and Evolution

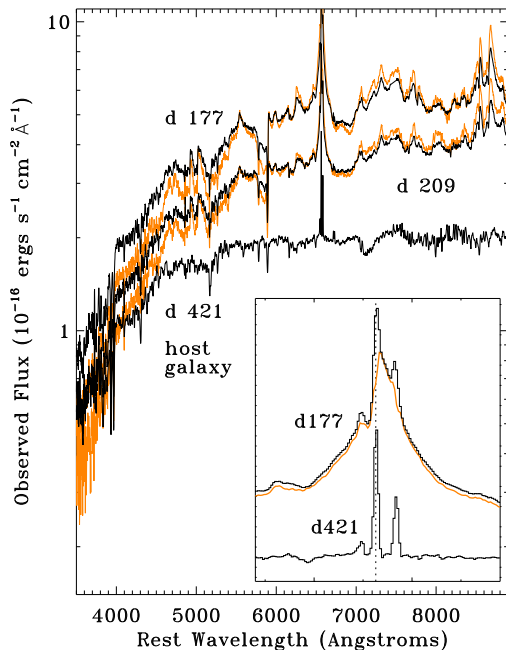


FIG. 3.— Late-time spectra of SN 2006gy illustrating background-subtraction issues. The day 421 spectrum is the extracted flux at the position of SN 2006gy at a time when the SN has faded beyond detectability. The day 177 and 209 spectra in black are the same as in other figures, where we have performed background subtraction by sampling the emission along the slit on each side of the SN. The gray (orange in the online edition) spectra are for the same dates, but where we have subtracted an additional amount of background-galaxy light using the day 421 spectrum (scaled to the same red flux level). These represent the most host-galaxy light that can be subtracted without causing erroneous narrow absorption at the position of nebular [N II] lines (see §2.2). The inset shows a detail of the spectral region around H α and [N II].

The overall spectral morphology of SN 2006gy can be characterized as a smooth blue continuum, convolved with a number of striking narrow and intermediate-width absorption and emission features (see Figure 4). Broad absorption features and broad P Cygni profiles typically seen in SN II-P atmospheres, with speeds of $\gtrsim 10^4$ km s $^{-1}$, are absent in the spectrum during the main light-curve peak. Rather, the broadest lines seen in the spectrum have speeds of ± 5000 km s $^{-1}$, where the line wings of H α join the continuum.

During the slow rise to maximum and the peak luminosity phase, SN 2006gy is characterized by a smooth blue continuum with few emission features besides the strong Balmer emission lines. It has few absorption features other than the interstellar Ca II and Na I lines. Shortly following peak luminosity, SN 2006gy takes on a distinct spectral morphology that changes little during the decline phase for ~ 100 days thereafter. The spectrum is punctuated by strong narrow emission and absorption features and intermediate-width absorption and emission. These produce interesting line-profile shapes with smooth red wings, but very sharp drops at $v = 0$ km s $^{-1}$ and blueward that are different from the smooth P Cygni profiles normally seen in SNe II. The most striking examples of this are the Fe II lines near 5000 Å (Figure 4).

The spectrum of SN 2006gy during this decline phase is relatively unique, but has some overlap with other SNe in various respects. The day 93 spectrum of SN 2006gy, which is exemplary of this phase, is compared with some

other SN II spectra in Figure 5.

SN 2005gj: Before the discovery of SN 2006gy, SN 2005gj was the most luminous SN known. It has been suggested to be a Type Ia explosion interacting with dense H-rich CSM, partly because its spectrum could be decomposed into a SN 1991T-like spectrum and a smooth polynomial (Aldering et al. 2005; Prieto et al. 2007). SN 2005gj is often grouped together with other luminous SNe II α like SNe 2002ic, 1997cy, and 1999E (Germany et al. 2000; Turatto et al. 2000; Rigon et al. 2003; Hamuy et al. 2003; Wang et al. 2004; Deng et al. 2004; Wood-Vasey et al. 2004; Chugai et al. 2004; Chugai & Yungelson 2004; Kotak et al. 2004; Benetti et al. 2006; Chugai & Chevalier 2007) because their spectra are similar, although the connection to SNe Ia has been questioned (Kotak et al. 2004; Benetti et al. 2006; Trundle et al. 2008).

Agnoletto et al. (2009) found an overall remarkable similarity between the spectrum of SN 2006gy and this class of objects, but our comparison with SN 2005gj in Figure 5 contradicts this assessment because we find that at a similar phase (93 vs. 98 days) their spectra are very different. SN 2006gy does not show the broad absorption features and undulations of the continuum that are seen in SN 2005gj (and its brethren SNe 2002ic, 1997cy, and 1999E), and its H α emission is much weaker relative to the continuum. As we note below, the similarity improves if one compares later phases of SN 2006gy to earlier phases of SN 2005gj, but such comparisons at different phases can be misleading, especially if one draws connections to the putative type of the underlying SN photosphere. In any case, with the high luminosity and long duration of SN 2006gy, emission from the underlying SN photosphere should make a negligible contribution to the total spectrum.

SN 2006tf: SN 2006tf is the second most luminous Type II α after SN 2006gy (Smith et al. 2008a). The similarity between spectra of SNe 2006gy and 2006tf (days 93 and 95, respectively) is better, as we noted in Paper I, although there is still some mismatch in blue spectral features. Relative to the continuum, Balmer-line emission is much stronger in SN 2006tf (note that the intensity scale in Figure 5 is logarithmic).

SN 2005gl: This SN II α deserves special mention, because so far it is the only SN II α for which a progenitor star has been detected in pre-explosion images (Gal-Yam & Leonard 2009). It is useful for comparison because it had a moderate luminosity, typical among SNe II α (Gal-Yam et al. 2007). Early-time spectra were of Type II α , but by about 2 months after explosion, the Type II α signatures weakened and the spectrum began to look more like Type II-P. The day 34 spectrum that we show in Figure 5 resembles that of SN 2006tf, despite the much lower luminosity of SN 2005gl. Gal-Yam & Leonard (2009) inferred that the progenitor star was a $L/L_{\odot} \approx 10^6$ LBV-like star that, in the year or so before the SN, had suffered an outburst with $\dot{M} \approx 0.03 M_{\odot} \text{ yr}^{-1}$. The event was therefore similar to the 1600 AD giant eruption of P Cygni (Smith & Hartigan 2006). The lower peak luminosity and relatively quick fading of CSM-interaction signatures in the spectrum of SN 2005gl are relevant to our study of SN 2006gy, because the precursor outburst that Gal-Yam & Leonard estimated, although extreme compared to normal winds, was tame compared to the

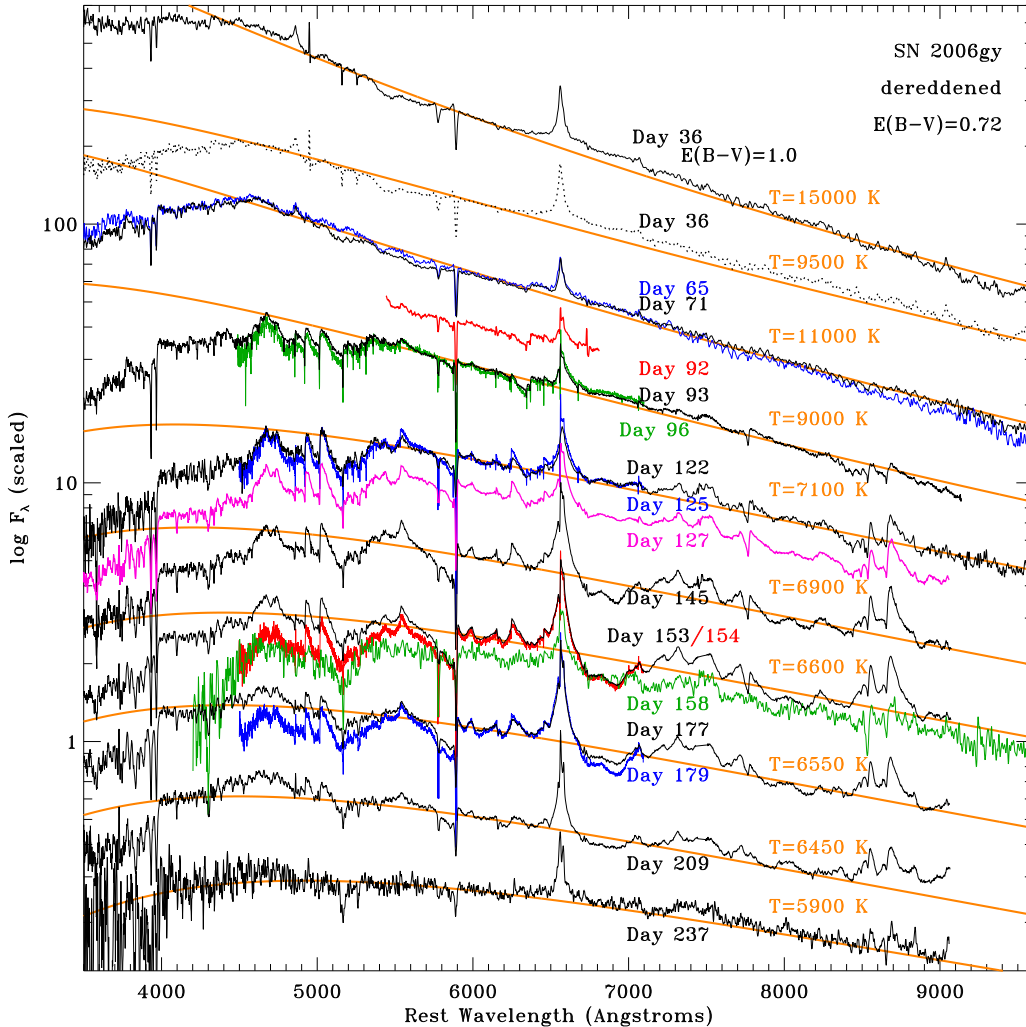


FIG. 4.— Same as Figure 2, but dereddened, plotted on a log scale, and scaled arbitrarily for display. The spectra have been dereddened by correcting for Galactic extinction of $A_R = 0.43$ mag and for the additional local extinction of $A_R = 1.25$ (Paper I), for a total $E(B - V) = 0.72$ mag. The day 36 spectrum is plotted twice: once with the same reddening correction as at other epochs (dotted) and once with a larger reddening correction (solid black). Representative blackbody temperatures are shown for comparison in orange.

precursor outburst needed for SN 2006gy.

SN 1994W: Perhaps the best overall similarity to the day 93 spectrum of SN 2006gy in Figure 5 is found with the spectrum of SN 1994W at day 89 (Chugai et al. 2004). The shape of the continuum and the amount of line blanketing at blue wavelengths show fairly good agreement. Both SNe share many of the same spectral features, although the narrow absorption and emission lines are stronger relative to the continuum in SN 1994W. A more detailed comparison to our higher-resolution day 96 DEIMOS spectrum of SN 2006gy is shown in Figure 6, where it is clear that most of the narrow line features are the same in both SNe, despite the different strengths. They are substantially narrower in SN 2006gy, with typical widths of $100\text{--}200\text{ km s}^{-1}$ instead of $800\text{--}1000\text{ km s}^{-1}$ in SN 1994W. Besides Balmer lines, most of these features are Fe II (Chugai et al. 2004). Chugai et al. interpreted this emission/absorption spectrum as arising from a combination of an expanding cold dense shell and dense pre-shock gas expanding at $800\text{--}1000\text{ km s}^{-1}$ to explain the narrow absorption features. Dessart et al. (2009), on the other hand, suggested that both com-

ponents arise in the recombination photosphere in the slowly expanding shell of SN 1994W, and that the broad wings arise primarily from electron scattering. Given the overall similarity to SN 2006gy, these aspects will resurface later.

SN 1995G and SN 1998S: These are two well-studied and prototypical SNe II_n with lower luminosity, faster spectral evolution, and much faster decline rates than those of SN 2006gy (i.e., they behaved more like SN 2005gl). Their spectra at 90–100 days after explosion do not resemble spectra of SN 2006gy at a comparable epoch because they have already become optically thin by that point (see Leonard et al. 2000; Fassia et al. 2001; Pastorello et al. 2002). At earlier times when it was still optically thick, however, the day 36 spectrum of SN 1995G has a strong smooth continuum with narrow absorption/emission features similar to SN 2006gy, although its Balmer emission lines are stronger. Similarly, on day 25 SN 1998S also has a strong smooth continuum, but in this case the Balmer lines are weaker than in SN 2006gy. This gives a qualitative illustration that the strength of H α is tied to the time evolution of the su-

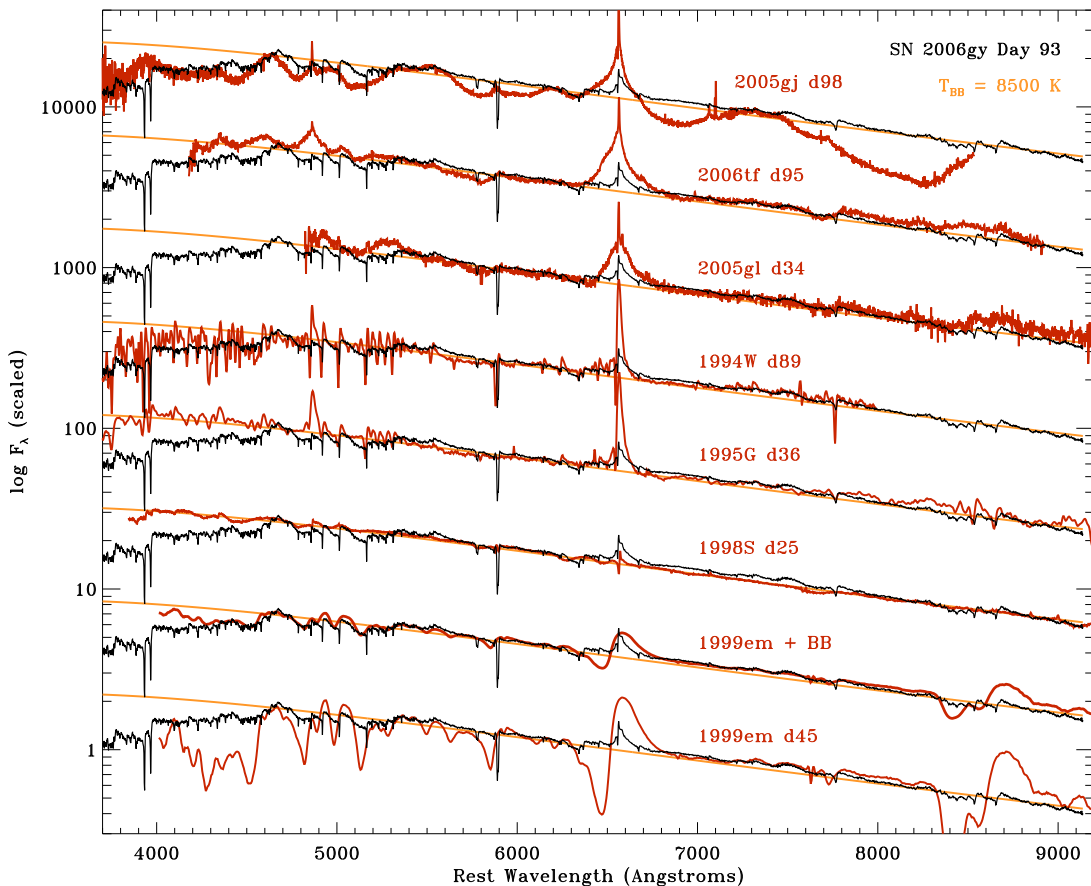


FIG. 5.— The day 93 LRS spectrum of SN 2006gy compared with spectra of several other SNe (red) and with a $T = 8500$ K blackbody (orange). The day 98 spectrum of SN 2005gj is unpublished from our spectral database, obtained on 2006 Jan. 01 with DEIMOS at the Keck Observatory. (In order to force a match to the continuum slope of SN 2006gy, this spectrum needed to be corrected for $E(B - V) = 0.35$ mag of reddening. This is an overcorrection compared to the actual value $E(B - V) = 0.12$ mag favored by Prieto et al. 2007.) The day 95 spectrum of SN 2006tf is from Smith et al. (2008a), but again with a high reddening correction. The day 34 spectrum of SN 2005gl is discussed in the Appendix. The day 89 spectrum of SN 1994W was obtained at Lick Observatory on 1994 Oct. 11 (see Chugai et al. 2004), and was corrected for $E(B - V) = 0.17$ mag (Sollerman et al. 1998). The day 36 spectrum of SN 1995G is from Pastorello et al. (2002), and the day 25 spectrum of SN 1998S is from Leonard et al. (2000). The day 45 spectrum of SN 1999em (bottom) is from Leonard et al. (2002) and is representative of a normal SN II-P photosphere. While this gives a poor match to the SN 2006gy spectrum by itself, the general shape of the spectrum matches better if we dilute the photospheric SN II-P spectrum with 2/3 of the flux contributed by a $T = 8500$ K blackbody. In all cases, but especially for SN 1999em, individual line profiles do not match because of different velocities in each object.

pernova’s optical depth. For SN 2006gy to maintain high optical depths for so long is remarkable among SNe IIn. We will discuss the $H\alpha$ line strength in more detail in §3.3 and 3.4. In SNe 1995G and 1998S, the blue/near-UV continuum is not as heavily affected by line blanketing as in SN 2006gy or SN 1994W.

SN 1999em: This is a prototypical SN II-P spectrum in mid-plateau. As noted earlier, one would obviously not expect the recombination photosphere within a rapidly expanding SN envelope to match the Type IIn spectrum of SN 2006gy, and indeed the very broad and deep absorption features in SN 1999em are unlike the narrow lines in SN 2006gy. However, we chose to display the spectrum of SN 1999em for the following reason: if we now *dilute* the photospheric spectrum of SN 1999em with a blackbody (second from bottom tracing in Figure 5), then we see a striking result. Ignoring the discrepant expansion speeds that cause broad lines in SN 1999em and narrow lines in SN 2006gy, the overall shapes of the two spectra match surprisingly well. This is especially true in the blue/near-UV regions, because this compos-

ite SN 1999em+blackbody matches the day 93 spectrum of SN 2006gy better than any SN IIn in Figure 5. This may suggest that the spectrum of SN 2006gy is generated by two components, such as a blackbody from ongoing CSM interaction combined with a recombination photosphere produced as radiation diffuses slowly out of an optically thick accelerated H envelope or shell (e.g., Smith & McCray 2007). Alternatively, it may mean that back radiation from the CSM interaction zone causes a muting of the line features via the “top-lighting” mechanism described by Branch et al. (2000). Diluting the observed spectrum in this way also provided the basis for comparing SN 2005gj to a SN Ia spectrum (Aldering et al. 2006; Prieto et al. 2007).

3.2. Continuum Evolution

The dereddened visual-wavelength continuum shape can be approximated adequately with a blackbody function, with the caveat that there is substantial line-blanketing absorption at blue wavelengths, particularly severe below ~ 4500 Å. No single temperature could ac-

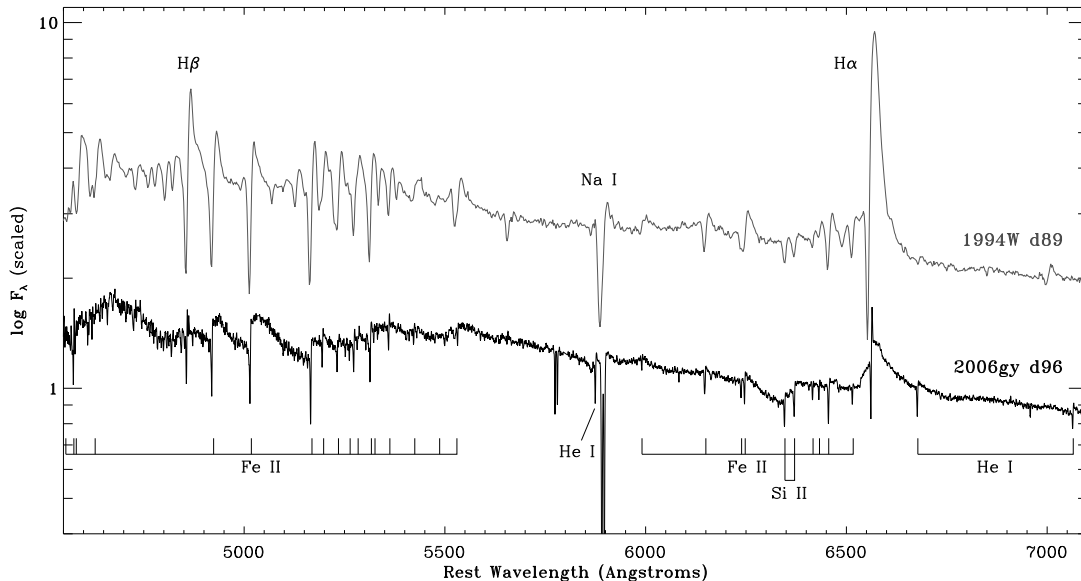


FIG. 6.— The dereddened day 96 high-resolution DEIMOS spectrum of SN 2006gy (black) compared to the day 89 spectrum of SN 1994W (gray) from Figure 5 (see Chugai et al. 2004), dereddened with $E(B - V) = 0.17$ mag (Sollerman et al. 1998). Several line identifications are marked. While many of the same lines can be seen in both SNe, especially in absorption, there are considerable differences in the relative emission-line strengths. Consider the different Balmer-line strengths and $H\alpha/H\beta$ emission-line intensity ratios, for example.

count for the spectral shape both above and below 4500 Å, so in Figure 4 we show blackbody curves (*orange*) which approximate the $\lambda > 4500$ Å continuum shape quite well, assuming that the decrease at short wavelengths is caused by additional absorption of the emitted blackbody spectrum. (The blue-wavelength flux at late times is quite uncertain and sensitive to the background subtraction.) This drop in flux at short wavelengths is common in SN II-P atmospheres, as noted above, and in some SNe II_n. A few representative temperatures for the continuum of SN 2006gy are shown in Figure 4, but all are listed in Table 1.

The evolution of the apparent blackbody temperature is plotted in Figure 7 (middle panel), where the solid black line is a smooth functional approximation to the time-dependent temperature, since our spectra irregularly and sparsely sample the temporal evolution. The temperature at early times (before day 50) is poorly constrained by our data because of the substantial reddening correction, and because of calibration issues with our day 36 spectrum as noted in §2. The day 36 estimate of the temperature has large uncertainty, so we consider two different cases for the early-time temperature evolution: a decline to lower temperatures around 10^4 K (solid curve) and a temporary rise to higher peak temperatures near 15,000 K (dashed). The lower temperature gives a better approximation of the continuum shape if we adopt the same reddening for all epochs (dashed day 36 spectrum in Figure 4). However, as shown in Figure 4, one can approximate the continuum shape somewhat better with a hotter 15,000 K blackbody if the day 36 spectrum is corrected for a larger reddening than the other epochs. This interpretation seems plausible given the high optical depths we expect in the inner CSM shell, as discussed later. We do not expect that the temperature was much above 15,000 K, since the day 36 spectrum shows no sign of the strong WR-like N III and He II features seen in the early phases of SN 1998S with temperatures above

20,000 K (Leonard et al. 2000).

These two treatments of the temperature yield somewhat different bolometric corrections and emitting radii at early times (Fig. 7), but have little impact on our overall interpretation. The solid curve would suggest a temperature evolution different from that of other SNe II_n, whereas the dashed curve with higher temperatures would make the temperature of SN 2006gy decline qualitatively similar to other SNe II_n. In either case, SN 2006gy takes much longer to cool, which is no doubt related to the extraordinary longevity of its peak luminosity phase. By day 150, the temperature settles to a floor at ~ 6500 K and remains nearly constant thereafter. The fact that this temperature agrees with the same late-time value inferred for less-reddened SNe II_n (like SNe 2005gj and 1998S in Fig. 7) could be taken to indicate that our assumed reddening value of $E(B - V) = 0.72$ mag is roughly correct. This temperature floor appears to be common among SNe II_n, whereas SNe II-P continue their decline to somewhat lower temperatures during their plateau phase.

These smooth curves approximating the temperature change of SN 2006gy are used to derive an approximate bolometric correction for the observed light curve in Figure 7 (top panel). The large filled circles correspond to the lower temperatures at early times (solid curve in temperature), whereas the small circles show what the corrected luminosity would be with the higher assumed temperature (dashed curve), although not taking into account the larger extinction correction implied by the higher temperature (see Fig. 4). Warmer temperatures before day 110 lead to an increase in our estimate of the bolometric luminosity (solid circles) and a slight shift in the time of peak luminosity from 70 days to about 60 days after the nominal explosion date. This bolometric correction affects the measured total radiated energy as well: in Paper I we found that the radiated energy integrated over the first ~ 200 days was 1.6×10^{51} erg. With the corrected L_{Bol} light curve in Figure 7, this es-

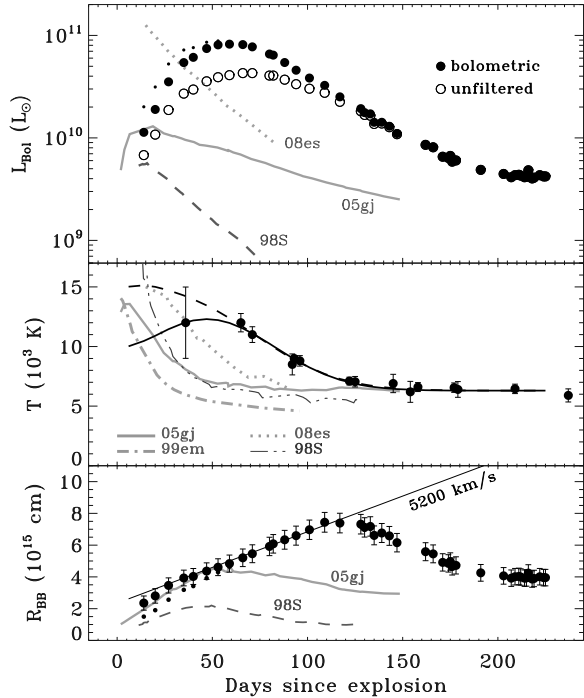


FIG. 7.— The light curve, apparent temperature, and implied blackbody photospheric radius of SN 2006gy. The unfilled points in the light curve are derived from unfiltered photometry from the 0.76 m Katzman Automatic Imaging Telescope (KAIT, at Lick Observatory) assuming zero bolometric correction (from Paper 1). The large filled and small filled circles in the light curve correspond to two different bolometric corrections that were applied, derived from the two temperature curves (solid and dashed, respectively) in the middle panel under two different assumptions about the early times (see text). Filled points plotted in the middle panel are apparent temperatures derived from observed continuum shapes in our dereddened spectra (Fig. 4; Table 1). The bottom panel shows the blackbody radius derived from the bolometric-corrected luminosity and the apparent temperature. Again, the large and small filled circles correspond to two different assumptions about the early-time temperature evolution. For comparison (gray), we also show bolometric luminosities and blackbody temperatures for SN 2008es (Miller et al. 2009a; Gezari et al. 2009), SN 1998S (Fassia et al. 2000), SN 2005gj (Prieto et al. 2007), and the prototypical Type II-P SN 1999em (Leonard et al. 2002). In the bottom panel, 5200 km s^{-1} corresponds to the full width at half-maximum intensity (FWHM) of the broad Gaussian component fit to the $H\alpha$ profiles described later. The inferred blackbody radii for SN 1998S and SN 2005gj are also shown.

time rises to roughly $(2.3\text{--}2.5) \times 10^{51}$ erg (the uncertainty is due to the uncertain temperature evolution at early times).

With these bolometric luminosity and temperature curves, we also derive the effective blackbody radius, $R_{\text{BB}}^2 = L/(4\pi\sigma T^4)$, plotted in the bottom panel of Figure 7. Again, the large solid points with error bars are for the lower temperatures at early times, and the small points show the derived radius for the higher temperatures. Differences between these two are minor, and do not much affect our discussion. The effective emitting radius of SN 2006gy behaves in a manner qualitatively similar to those of other SNe II in that R_{BB} increases steadily for a time, reaching a peak and then decreasing again. For SN 2006gy, this turnover occurred much later than in any other SN — R_{BB} turned over around day 115, whereas it occurred much earlier at day ~ 50 for both SNe 1998S and 2005gj (Fassia et al. 2000; Prieto et al. 2007), and at day 70–80 in SN 2006tf (Smith et al.

2008a). In all cases, the turnover of R_{BB} was well after the time of the supernova’s peak luminosity.

Presumably this peak represents a critical transition point when the shell starts to become optically thin. In the case of SNe II-P, this occurs as the H-recombination photosphere recedes backward through the geometrically thick expanding H envelope of the star. This marks a clear division in radius between the inner optically thick ionized ejecta and the outer recombined transparent ejecta. In SNe II in, however, one expects the post-shock shell to form a geometrically very thin layer (a “cold dense shell,” or CDS; see Chugai et al. 2004), because the post-shock layer collapses due to radiative cooling. In that case, the turnover and subsequent decrease of R_{BB} is misleading, because R_{BB} decreases more than the expected shell thickness, which should be much less than 10% of R_{shell} . Also, apparent velocities measured in the $H\alpha$ line do not decrease during this time.

Motivated by similar observations of the luminous SN 2006tf, we (Smith et al. 2008a) explained this behavior in SNe II in as follows: the derived value of R_{BB} is not the true radius of the emitting surface in the cold dense shell, but rather, $R_{\text{BB}}^2 = \zeta R_{\text{shell}}^2$. The true physical radius of the shell, R_{shell} continues to increase with time, but ζ is a dilution factor representing the fractional geometric covering area of the shell ($\zeta \leq 1$, decreasing with time). The post-shock shell is able to continue producing continuum radiation with a constant effective temperature of 6000–6500 K, despite its reduced effective opacity, because it is clumpy; small clumps remain ionized and optically thick longer, whereas less dense inter-clump regions gradually recombine and become transparent. One expects the CDS to be severely clumped because of Rayleigh-Taylor instabilities at the contact discontinuity. Limb-brightening effects may also be important in determining ζ .

The rate at which R_{BB} increases with time during early phases before this transition occurs (between days 40 and 120) seems to roughly match an expansion speed of $\sim 5,200 \text{ km s}^{-1}$ (solid line in Fig. 7). This speed is taken from the broadest Gaussian matched to the $H\alpha$ emission profiles, which seem to imply constant expansion speeds at all times, as we discuss below in §3.3. $H\alpha$ continues to indicate roughly the same expansion speeds after the turnover in R_{BB} at day 115, when one expects that high optical depth effects like electron scattering wings will be less influential. The expansion speed of the photosphere seemed to be somewhat faster before day 25, but unfortunately our data do not provide good constraints because of uncertainties associated with the apparent temperature at early times. The radius around day 25 of $\lesssim 3 \times 10^{15}$ cm or $\lesssim 200$ AU roughly matches the expected initial radius of the highly opaque CSM shell inferred by Smith & McCray (2007), who claimed that it may have taken a few weeks for the SN to traverse this shell and become luminous.

3.3. The Broad $H\alpha$ Line Profile

The evolution of the broad to intermediate-width component of $H\alpha$ is a key diagnostic of the CSM interaction in SNe II in, and will be discussed in some detail in the following sections. We show a time series of the $H\alpha$ profile of SN 2006gy in Figure 8, and we display the line profiles at several epochs obtained with high resolution

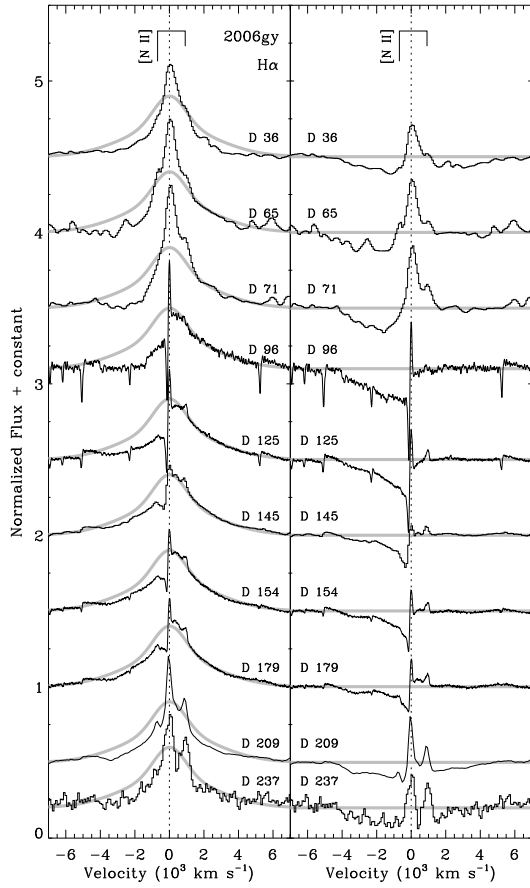


FIG. 8.— $H\alpha$ line profiles in SN 2006gy at several epochs (not including redundant spectra with lower resolution). The left side shows the observed profile normalized to the continuum level, overplotted with a symmetric Gaussian curve in gray. This is a sum of two Gaussians with a FWHM of 5200 and 1800 km s^{-1} , each with the same peak intensity. The expected positions of $[N \text{ II}] \lambda\lambda 6548, 6583$ are shown. The right side shows the same $H\alpha$ profiles with the symmetric Gaussian subtracted to emphasize the blueshifted broad absorption. The first three spectra at days 36, 65, and 71 have lower spectral resolution.

in Figure 9.

Caveats to keep in mind for the discussion below are the following. Our first three spectra on days 36, 65, and 71 were obtained with the Kast spectrograph at Lick Observatory, and have lower spectral resolution than the Keck/DEIMOS and LRIS data. This alters the appearance of the narrow emission/absorption components and the transition between the narrow and broad components on those dates in Figure 8. The red side of the $H\alpha$ line is affected by $[N \text{ II}] \lambda 6583$ emission to varying degrees, and the blue side by $[N \text{ II}] \lambda 6548$ to a lesser degree; the positions of these lines relative to the $H\alpha$ systemic velocity are marked in Figures 8 and 9. The $H\alpha$ profile is also affected by weaker broad and narrow lines of He I and Fe II, as noted in Paper I, whereas the blue wing of the line is depressed by varying amounts of broad blueshifted $H\alpha$ absorption. For all profiles in Figure 8, we have normalized to the smooth continuum level (see Fig. 4) and scaled the emission-line strength in order to compare profile shapes. We do not plot the $H\alpha$ profiles on days 92, 93, 122, 127, 153, 158, and 177, because they are redundant for our purposes, superseded by higher-resolution DEIMOS data obtained within a few days.

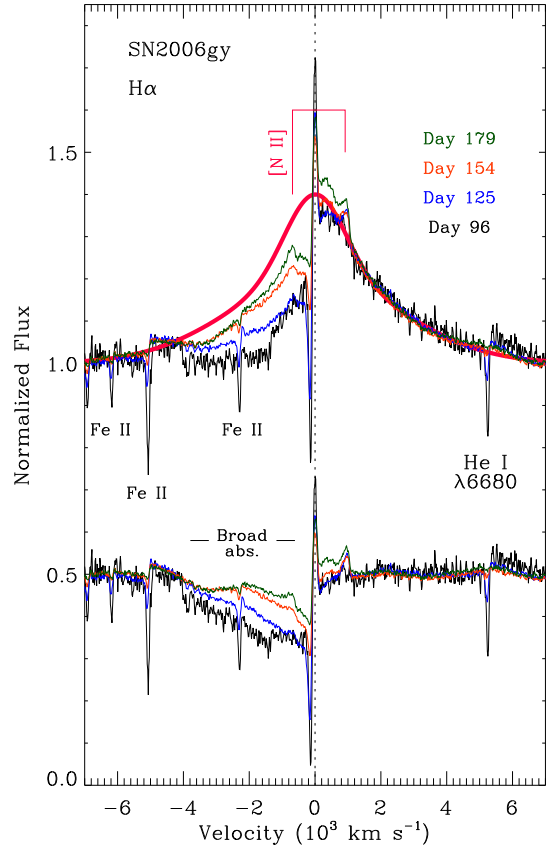


FIG. 9.— The broad component of the $H\alpha$ line profile in SN 2006gy from the four DEIMOS spectra obtained at high resolution, normalized to the same continuum level and overplotted. The blue wing of $H\alpha$ undergoes strong and systematic variations, with the absorption weakening with time, while the red wing remains remarkably constant. The expected positions of $[N \text{ II}] \lambda\lambda 6548, 6583$ are shown. The thick magenta curve is the sum of two symmetric Gaussians with a FWHM of 5200 and 1800 km s^{-1} , as in Fig. 8. The lower set of tracings are the same as the upper profiles, but with this Gaussian subtracted, as in Fig. 8.

To provide a fiducial profile for comparison, we plot each $H\alpha$ profile on top of a symmetric Gaussian, shown in gray in Figure 8 and in magenta in Figure 9. This symmetric profile is the sum of two Gaussians with equal intensity and FWHM values of 5200 km s^{-1} and 1800 km s^{-1} . It is not necessarily the best fit to the profile on any specific date, but it gives an adequate match to the red wing for most epochs except as noted below. In addition, for the right-hand panel in Figure 8 and for the lower set of tracings in Figure 9, we show the residual profile after subtracting away this symmetric Gaussian in order to emphasize changes in the broad blueshifted $H\alpha$ absorption.

3.3.1. The Pre-Maximum $H\alpha$ Profile

Our earliest spectrum — the only one obtained while SN 2006gy was still on its slow rise to maximum luminosity — was obtained on day 36. This is an unfortunate consequence of the fact that the SN was not discovered until about 29 days past our adopted explosion date. (Upper limits and photometry before that time were extracted from pre-discovery data.) Also, SN 2006gy was initially thought to be an active galactic nucleus; its peculiar SN nature was not realized until relatively late (see Paper I and references therein).

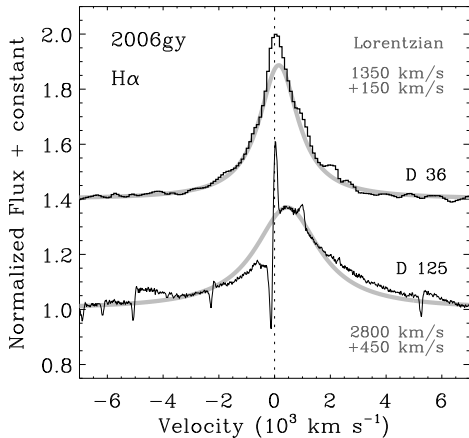


FIG. 10.— The $H\alpha$ profiles on days 36 and 125, compared to Lorentzian profiles. The day 36 spectrum can be adequately represented by a single Lorentzian with $\text{FWHM} = 1350 \text{ km s}^{-1}$ and with its centroid redshifted by 150 km s^{-1} , ignoring some unresolved narrow emission. A Lorentzian with $\text{FWHM} = 2800 \text{ km s}^{-1}$ and with its centroid redshifted by 450 km s^{-1} does not give a very good representation of the day 125 line profile, or the $H\alpha$ profile at any other epoch after the time of peak luminosity.

As discussed below, the broad Gaussian curve in Figure 8 gives an adequate match to the red wing of $H\alpha$ for most epochs, with a clear exception being the first spectrum on day 36. The broadest component on day 36 is substantially *narrower* than the Gaussian curve; consequently, subtraction residuals show a broad deficit in the redshifted wings.

Instead, the broad $H\alpha$ wings on day 36 are better matched by a single Lorentzian profile, with $\text{FWHM} = 1350 \text{ km s}^{-1}$ and with its centroid redshifted by $+150 \text{ km s}^{-1}$ (Fig. 10). This is not true for any epoch after day 90, when a single Lorentzian that fits the broad line wings and core would significantly underestimate the wings at $\pm 1000\text{--}3000 \text{ km s}^{-1}$, and would require a net redshift of $+450 \text{ km s}^{-1}$ (an example of such a profile plotted with the day 125 spectrum is shown in Figure 10). In addition to the broad Lorentzian, the line has an unresolved narrow Gaussian component that contributes $\sim 7\%$ of the total $H\alpha$ luminosity.

A similar result was found for the $H\alpha$ profile in early spectra of SN 1998S, where Leonard et al. (2000) showed that on day 5 it was well fit by a broad Lorentzian plus an unresolved component that contributed 20–25% of the line luminosity. Chugai (2001) proposed that this profile arises from an intrinsically narrow $H\alpha$ line that is broadened by collisions with thermal electrons in an opaque circumstellar shell outside the photosphere. The Lorentzian wings arise from multiple electron scattering, whereas the unresolved narrow component is direct emission. A similar model may explain the early-time $H\alpha$ emission from SN 2006gy. In this interpretation, the net $+150 \text{ km s}^{-1}$ redshift of the Lorentzian centroid corresponds to the expansion speed of the CSM at these inner radii (see Chugai 2001). A rough estimate of the scattering envelope’s optical depth outside the photosphere, τ , is given by $U = (1 - e^{-\tau})/\tau$, where U is the ratio of the unscattered narrow component to the total line luminosity. For SN 2006gy on day 36 we measure $U \approx 0.07$, yielding $\tau \approx 15$. The pre-SN envelope is evidently highly

opaque.

The FWHM of this Lorentzian component on day 36 is only 1350 km s^{-1} , which is much slower than the necessary expansion speed of $\sim 5000 \text{ km s}^{-1}$ corresponding to $d(R_{\text{BB}})/dt$ in Figure 7. If anything, the true expansion speed of the photosphere should have been *even faster* before day 36. Thus, at this early phase, the line wings cannot be caused by electron scattering within the rapidly expanding CDS itself, as suggested for SN 1994W by Dessart et al. (2009), although this effect may play a role at later epochs (see below). Since no broader components are seen at early times, we must conclude that the $H\alpha$ profile on day 36 does not trace the kinematics of the SN. Rather, it seems likely that the opaque photosphere occurs *outside* the forward shock, as a radiative precursor ionizes the relatively slow and extremely dense pre-shock CSM. This opaque ionized region hides the underlying SN kinematics from our view, so that the broad line profiles at early times are due entirely to Thomson scattering of narrow lines formed in the CSM, whereas the rising luminosity and increase in R_{BB} at early times is due entirely to a rapidly expanding ionization front. The dereddened $H\alpha/H\beta$ ratio of ~ 2.9 on day 36 (Table 1) seems consistent with this interpretation. This radiation cannot escape directly from the post-shock zone, but must diffuse out through the opaque envelope, as suggested by Smith & McCray (2007) to explain the slow rise to maximum of SN 2006gy.

Altogether, the spectrum of SN 2006gy in the time period when it was still slowly rising to maximum luminosity can be characterized by a blackbody photosphere expanding within an opaque electron-scattering circumstellar shell. This was also the case for SN 1998S, but only at the very earliest times up to day 5. The much longer duration of this phase in SN 2006gy is yet another testament to the extraordinarily dense and extended pre-SN envelope. It is unfortunate that additional spectra were not obtained during this early phase; they would have allowed us to constrain the density structure in the inner parts of this circumstellar shell in more detail.

3.3.2. Nearly Constant-Velocity Line Wings

A striking conclusion from examination of Figures 8 and 9 is that after the time of peak luminosity, the profile of the broad emission component of $H\alpha$ is remarkably constant. Most importantly, the speed does not decrease substantially as the SN emits most of its radiation.

To be more precise, the line width does change somewhat with time – in fact, the line width *increases* with time after peak luminosity (Fig. 9) – but this is primarily because varying amounts of P Cygni absorption alter the blue wing, as discussed below. Examining the red wing of $H\alpha$ exclusively, however, we see *no significant changes in the underlying emission profile shape from the time of peak luminosity onward*. This is especially clear in the residuals after the same symmetric Gaussian has been subtracted from each profile (Figs. 8[right] and 9). Except for a small bump around He I $\lambda 6678$ and narrow emission from [N II], the red-wing subtraction residuals are essentially flat for all epochs after day 36. In particular, we see no evidence for a change in expansion speed before, during, or after the time when R_{BB} turns over (Fig. 7) in transition to the optically thin phase.

Observations of other SNe IIn tend to show declining

FWHM for the post-shock gas during high-luminosity phases, as for SN 1988Z in its first year (Turatto et al. 1993; Chugai & Danziger 1994; Aretxaga et al. 1999), whereas models predict a sharp decline in the CDS velocity around the time of peak luminosity (Chugai 2001; Chugai & Danziger 2003; Chugai et al. 2004). A nearly constant expansion speed for the CDS is a product of these models at later times, however, in cases where most of the deceleration has already occurred at early times near peak luminosity when the blast wave overtook a dense shell, as suggested for SN 1994W and SN 1995G (Chugai & Danziger 2003; Chugai et al. 2004). Subsequently, a constant shell speed is seen as the forward shock takes on self-similar expansion through a $\rho \propto r^{-2}$ wind. At early times near peak luminosity, however, models predict that the CDS emitting the intermediate-width $H\alpha$ line decelerates as the post-shock cooling zone is mass loaded by the CSM gas swept up by the forward shock. As we have argued above, this early deceleration phase was hidden from our view by the opaque CSM that surrounded SN 2006gy.

Thus, in principle, a constant expansion speed of the post-shock shell in SNe IIn is understandable, but the case of SN 2006gy is problematic because of the energy budget. SN 2006gy remained at high luminosity for an astonishingly long time, emitting more than 10^{51} erg of visual light while its expansion speed remained roughly constant. One expects 10^{51} erg to be a substantial fraction of the total available kinetic energy of the explosion, so unless the ejecta of SN 2006gy are extremely massive and energetic, the lack of deceleration as this energy escapes by radiation is puzzling, as we noted in Paper I. Furthermore, after day ~ 120 when R_{BB} retreats and the shell begins to become optically thin, the luminosity is still much higher than one can expect from the level of CSM interaction inferred from the $H\alpha$ or X-ray luminosities, as discussed below. A possible resolution to this paradox, as suggested by Smith & McCray (2007), is if the expected deceleration occurs at earlier opaque phases when the radiation cannot escape, converting shock energy into thermal energy, and emitting after a delay because that radiation must diffuse out of the opaque shell.

While the velocities up to 5200 km s^{-1} that we infer from the broad $H\alpha$ component are consistent with the rate of increase of R_{BB} , we cannot rule out the possibility that other factors affect the line profile. Namely, Dessart et al. (2009) suggested that in the case of SN 1994W, which appears to have similar line widths and a similar overall spectral morphology to SN 2006gy, the line width was generated largely by incoherent electron scattering within the $H\alpha$ -emitting shell itself. SN 2006gy is a good candidate for investigating high optical depth effects, and further hydrodynamic and radiation-transfer models are encouraged. Since the photosphere radius must be increasing at speeds near 5000 km s^{-1} that are comparable to the expected electron-scattering wings, however, one expects that the kinematic and electron-scattering wings are intermixed and hydrodynamics cannot be treated separately from radiation transfer.

Our analysis of the $H\alpha$ line profiles is different from that of Agnoletto et al. (2009), who find a broad Gaussian component in $H\alpha$ with $\text{FWHM} = 9000 \text{ km s}^{-1}$. Their conclusion was based on a Gaussian decomposi-

tion of the $H\alpha$ profile seen in a low-resolution, late-time (day 173) spectrum. Our spectra show that at such late times, the spectral regions on either side of $H\alpha$ are affected by additional broad absorption features unrelated to $H\alpha$, and these can mimic the appearance of broader line wings. On the red wing of $H\alpha$, there is an absorption feature below the nominal continuum level at $6700\text{--}7000 \text{ \AA}$, and the blue wing of $H\alpha$ is affected by a complex blend of broad Si II absorption and several Fe II emission features. Choosing the trough of this absorption as the continuum gives an underlying continuum level and slope that are inconsistent with the rest of the spectrum across a broader wavelength range. This red absorption feature is seen even more clearly in the cases of other luminous SNe IIn like SN 2005gj (Fig. 5). Thus, our data show no evidence for an $H\alpha$ emission component broader than 5200 km s^{-1} that might be attributed to fast underlying SN ejecta. SN ejecta moving at 9000 km s^{-1} would have already reached and overtaken the reverse shock (with $R \leq R_{\text{BB}}$; Fig. 7) by day ~ 70 when the post-shock region was still opaque. All ejecta reaching the reverse shock after that point must be slower unless the ejecta and CSM are severely asymmetric.

3.3.3. Broad Blueshifted Absorption

SN 2006gy is quite extraordinary among SNe IIn in that its intermediate-width $H\alpha$ line from the post-shock shell also exhibits significant blueshifted absorption. Excluding narrow absorption from pre-shock CSM gas, most SNe IIn, by contrast, show more symmetric $H\alpha$ wings, with some key examples being SN 1988Z (Turatto et al. 1993), SN 1997eg (Salamanca et al. 2002; Hoffman et al. 2008), SN 1997cy (Turatto et al. 2000), SN 1999E (Rigon et al. 2003), and SN 2006tf (Smith et al. 2008a). The broad P Cygni absorption in SN 2006gy is, however, reminiscent of weaker broad absorption at similar speeds in SN 1994W around day 50 (Chugai et al. 2004; Dessart et al. 2009) and SN 1998S at 2–4 weeks (Fassia et al. 2001). In Paper I we noted that this broad blueshifted absorption extends out to roughly -4000 km s^{-1} , seen most clearly in the day 96 profile when a sharp blue edge is apparent. Here we find that some broad P Cygni absorption is present at most epochs.

In Figures 8 and 9, the nature of this flux deficit as absorption (as opposed to line asymmetry) is particularly clear when we subtract away a symmetric Gaussian profile. Interestingly, these Gaussian-subtracted profiles look similar to the $H\alpha$ profile of SN 1998S observed on day 17.7 (Fassia et al. 2001), which showed broad absorption out to -6000 km s^{-1} and a narrow P Cygni component, but no broad emission. In SN 2006gy, residuals show consistent blueshifted absorption at 0 to -4000 km s^{-1} . Admittedly, the strength of this P Cygni absorption on day 36 is unclear, as we have argued above that the line can also be fit well with a narrower Lorentzian profile that has a redshifted centroid as a natural consequence of electron scattering in an expanding wind. The remaining epochs, however, cannot be explained in this way because their red-wing subtraction residuals are flat.

After day 36, the relative strength of this broad P Cygni absorption changes with time compared with the emission profile. It seems to increase during and immediately after peak luminosity, being strong from days 71 to 125. The absorption is strongest in the day 96 spec-

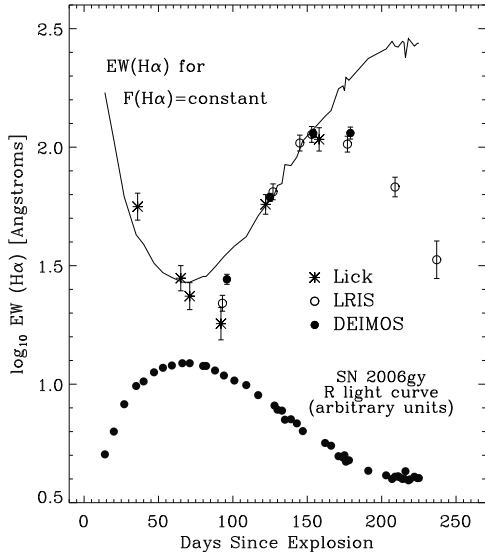


FIG. 11.— Observed $H\alpha$ equivalent width in spectra of SN 2006gy. The light curve is shown for reference at the bottom, and the solid curve shows what the $H\alpha$ equivalent width would be if the $H\alpha$ emission-line flux were constant and all that changed were the underlying continuum luminosity. The three plotting symbols refer to measurements with three different instruments (see Table 1).

trum, and weakens thereafter as the SN fades (Fig. 9). Because the broad blueshifted absorption steals a substantial fraction of the total line flux at some epochs, it is relevant to our interpretation of the $H\alpha$ equivalent width and line luminosity (§3.4).

Although the *strength* of the broad blueshifted absorption changes with time, the total *range* of velocities out to roughly -4000 km s^{-1} remains constant from the time of peak luminosity until our last spectrum over 150 days later. This constant speed seen in absorption is consistent with the unchanging speeds deduced from the red wing of $H\alpha$, supporting the notion that the CDS and blast wave of SN 2006gy continue to expand at constant speed. The maximum speed of absorbing material along our sight-line is 4000 km s^{-1} , somewhat less than the FWHM of the broadest Gaussian emission component and less than the nominal expansion speed indicated by the growth of R_{BB} in Figure 7. The significance of this difference is not immediately clear, and may require detailed radiative transfer models of the line profiles. For example, it is possible that the true expansion speed is 4000 km s^{-1} , while the broader emission wings out to $\pm 6000 \text{ km s}^{-1}$ are due to electron scattering.

Interestingly, the broad blueshifted absorption never dips below the continuum level. At its deepest point on day 96, the blueshifted absorption floor is flat at roughly the continuum level. This may suggest primarily self-absorption of the $H\alpha$ line wings and not necessarily absorption of the continuum.

3.4. The Total $H\alpha$ Equivalent Width and Luminosity

The measured $H\alpha$ equivalent width and line luminosity are shown in Figures 11, 12, and 13, and are discussed below. The measured $H\alpha$ equivalent width has several potential sources of error.

First, we are comparing data obtained with different telescopes, instruments, and (most importantly) slit

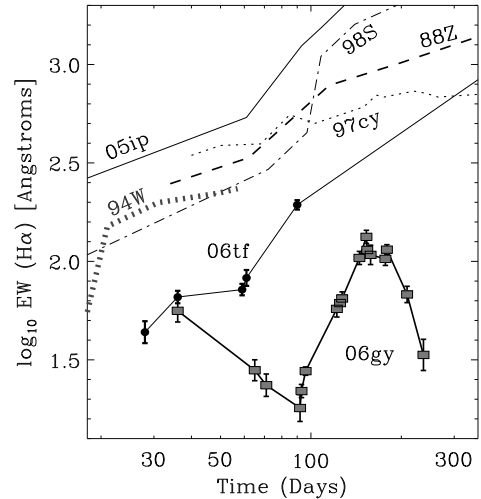


FIG. 12.— Observed $H\alpha$ equivalent width in spectra of SN 2006gy from Figure 11 compared to several other SNe (compiled by Smith et al. 2008a, 2009a).

widths. This is not a severe problem at early times when the SN is bright, but it can be problematic at late phases. Figure 11 shows the equivalent width plotted with different symbols corresponding to the three spectrographs we used. Spectra obtained at Lick Observatory have the largest slit width, so these equivalent width measurements are likely to have the largest systematic error because of the difficulty in subtracting background light. Overall, we found that the LRIS and DEIMOS measurements were very consistent, whereas the Lick measurements at comparable epochs showed larger variation. For this reason, we adjusted the equivalent widths of the Lick measurements to correct for partial contamination by $10^{-15} \text{ erg s}^{-1} \text{ cm}^{-2} \text{ \AA}^{-1}$ of galaxy continuum light in the slit, which brought the late-time equivalent width into agreement with the LRIS and DEIMOS values. This is justified by the similar line luminosities at those times, which are not altered by the continuum level.

Second, the $H\alpha$ profile is complex, with several adjacent overlapping line features that change with time. For example, at late times, the red wing of $H\alpha$ descends into a broad absorption feature at $6700\text{--}7000 \text{ \AA}$, which alters the underlying continuum level. The blue wing is plagued by broad P Cygni absorption and by Fe II and Si II lines. These complexities are exacerbated by the different spectral resolutions of different instruments. We aimed to consistently measure the $H\alpha$ equivalent width and flux over a wavelength range of $6400\text{--}6700 \text{ \AA}$, although the effects noted above introduce uncertainty in the underlying continuum level at 5–10%. Equivalent width and flux measurements listed in Table 1 reflect the total $H\alpha$ line, including intermediate-width and narrow components. We made no correction for Fe II and He I lines included in the sampled wavelength range.

3.4.1. $H\alpha$ Equivalent Width

The $H\alpha$ equivalent width changes dramatically as SN 2006gy evolves, decreasing rapidly during the first 100 days, and then rising steeply for the next ~ 50 days, only to drop off again at late times (Fig. 11). The $H\alpha$ equivalent width appears to be roughly anticorrelated with

the SN luminosity, with the minimum equivalent width occurring near peak. The solid line in Figure 11 demonstrates what the equivalent width would be if the $H\alpha$ line luminosity were to remain constant with time. This gives a fairly good match to the observed behavior during the main light-curve peak, considering that the $H\alpha$ line is affected by strong P Cygni absorption that diminishes the equivalent width by varying amounts with time. This implies that the production of $H\alpha$ is not closely tied to the engine that drives the continuum luminosity of SN 2006gy.

The $H\alpha$ equivalent width of SN 2006gy is compared to that of several other SNe IIn in Figure 12; we find that SN 2006gy behaves unlike any of them. All SNe IIn show a consistent trend of steadily increasing $H\alpha$ equivalent width with time, presumably due to steadily decreasing optical depth in the post-shock shell. Unlike the case in other SNe IIn, the $H\alpha$ equivalent width of SN 2006gy plummets at first, rises sharply, and then drops off again. We conjecture that during early phases, the photosphere is ahead of the shock, but the amount by which the photosphere leads the shock decreases with time. The difference compared to other SNe IIn is probably a consequence of SN 2006gy’s much slower rise to peak luminosity because of much higher optical depths — in other words, similar phases in other SNe IIn may occur quickly at early times and may be rarely observed.

The subsequent rise in equivalent width during intermediate phases (days 90–150) seems consistent, at least for this brief interlude, with the behavior of other SNe IIn. This phase starts just before the critical time when R_{BB} turns over and the shocked shell starts to become effectively optically thin. This seems to imply that during this phase, radiation from CSM interaction in SN 2006gy behaves like in standard SNe IIn because by this time the post-shock layer is becoming sufficiently optically thin to cool directly.

However, in addition to behaving differently with time, the measured $H\alpha$ equivalent width of SN 2006gy is also much lower than that of any other SN IIn in Figure 12. At its time of maximum luminosity ~ 70 days after explosion, the $H\alpha$ equivalent width of SN 2006gy is 20 times lower than in a standard SN IIn like SN 1998S, and almost a factor of 10 lower than in the very luminous SN IIn 2006tf. This implies that direct cooling from ongoing CSM interaction contributes only a fraction of the total luminosity. (Note that the weakness or lack of He I suggests that the H abundance is not particularly low.)

3.4.2. $H\alpha$ Line Luminosity

Examination of the intrinsic $H\alpha$ luminosity sheds additional light on the problem (Fig. 13). In agreement with our conjecture from the equivalent width, the $H\alpha$ line luminosity stays roughly constant during the first 150 days: it does not change by more than a factor of 2 while the SN continuum luminosity brightens and fades by a factor of 10. The relative minimum around day 100 coincides with a time when the broad P Cygni absorption was particularly strong.

Figure 13 reveals that SN 2006gy has similar $H\alpha$ line luminosity compared to other luminous SNe IIn. The total $H\alpha$ luminosity hovers around $(2\text{--}3) \times 10^{41}$ erg s^{-1} , comparable to that of SN 1997cy and SN 2006tf. This

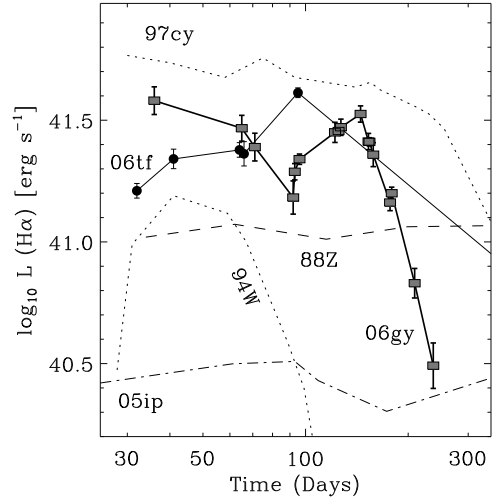


FIG. 13.— Observed $H\alpha$ luminosity of SN 2006gy, corrected for Galactic and local extinction, compared to that of several other SNe IIn (from Smith et al. 2008a, 2009a).

is somewhat surprising, as SN 2006gy was a factor of 5–10 more luminous in the continuum. Together, then, the $H\alpha$ equivalent width and luminosity imply that the engine that generates the $H\alpha$ line luminosity (probably direct cooling from post-shock gas at late times) may not be the dominant source of the peak continuum luminosity. One likely solution is that the continuum luminosity includes a contribution from shock-deposited thermal energy that occurred earlier and must diffuse out of the opaque shocked shell after a delay (Smith & McCray 2007).

At late times after day 150, both the equivalent width and total $H\alpha$ luminosity drop. The closest behavior to this is in SN 1994W, which also showed a sharp drop, while SN 1997cy dropped off at later times as well. As in the case of SN 1994W (Chugai et al. 2004), the most likely explanation is that the blast wave reached an outer boundary of a circumstellar shell. This suggests, therefore, that the CSM had a sharp density drop at a radius of roughly 10^{16} cm or ~ 600 AU. Again, however, we see that the continuum luminosity did not exhibit such a sharp drop at that time, suggesting that ongoing CSM interaction was only contributing a portion of the total continuum luminosity.

3.4.3. The $H\alpha/H\beta$ Line Ratio

Finally, in Table 1 we also list the dereddened $H\alpha/H\beta$ line intensity ratio. The first few epochs have reliable measurements, but after the time of peak luminosity the ratio becomes less certain: $H\beta$ becomes extremely faint and blended with neighboring broad features, so the continuum level is unclear. Also, it develops deep self absorption that sometimes overwhelms the emission component. At late times, it is difficult to discern any intermediate-width $H\beta$ component at all. $H\beta$ emission is dominated at late times by a narrow feature from the pre-shock CSM. By contrast, the narrow pre-shock CSM component of $H\alpha$ typically contributes less than 10% of the total line flux.

At early epochs before and during maximum luminosity, the $H\alpha/H\beta$ line ratio is roughly consistent with

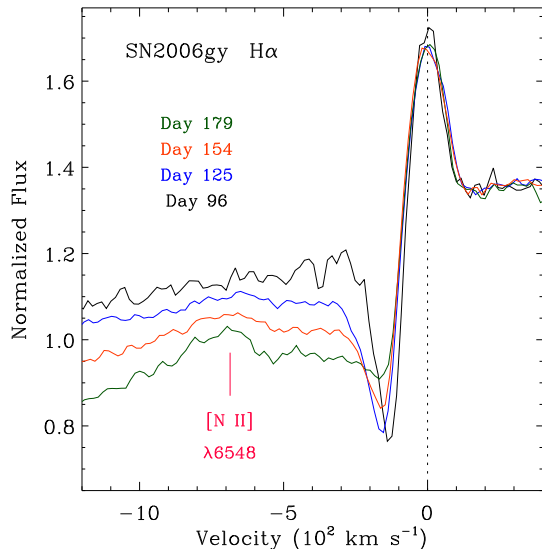


FIG. 14.— The narrow component of the $H\alpha$ line profile in SN 2006gy on the four DEIMOS epochs observed at high resolution, normalized to the same continuum level. The narrow blueshifted $H\alpha$ absorption gets weaker but broader with time.

recombination, supporting the notion that the line is formed largely by photoionization of pre-shock circumstellar gas and subsequent line broadening by electron scattering. At later epochs the $H\alpha/H\beta$ line ratio is extremely high, with all values well above 30, as seen in late-time spectra of SNe II α with strong interaction like SN 1988Z and SN 2006tf (Turatto et al. 1993; Smith et al. 2008a). Even taking into account the large uncertainties, this clearly suggests collisional excitation in a shock, and therefore implies that CSM interaction dominates the $H\alpha$ luminosity during the decline from maximum. A very similar growth in the $H\alpha/H\beta$ ratio was seen in SN 2005gj (Prieto et al. 2007), although the transition from low to high values occurred more quickly there.

The onset of high $H\alpha/H\beta$ ratios (> 30) after day 100 appears to coincide with the time when R_{BB} turns over and the $H\alpha$ equivalent width begins to grow, presumably marking the point when the swept-up shell starts to become optically thin. *From this time onward, the optically thin $H\alpha$ luminosity should therefore be a reliable indicator of the strength of CSM interaction and a tracer of the mass-loss rate of the progenitor star at large radii.* This is a key point, since the $H\alpha$ luminosity is lower than one expects from the continuum luminosity even at those late phases.

3.5. The Narrow $H\alpha$ Line Profile

In addition to the broad $H\alpha$ component discussed above, SN 2006gy also has strong narrow $H\alpha$ emission from the photoionized but unshocked CSM. In Paper I we presented a high-resolution spectrum of $H\alpha$ on day 96, which revealed a narrow blueshifted P Cygni absorption line as well. This component indicated outflow speeds of $\sim 260 \text{ km s}^{-1}$ in the pre-shock CSM. If this is attributed to the wind speed of the progenitor star, it suggests an escape velocity comparable to that expected in blue supergiants. If it is associated with an explosive pre-SN ejection, it is reminiscent of the speeds seen from LBV eruptions (see Paper I). It is much faster than speeds expected for a red supergiant (RSG), and much slower

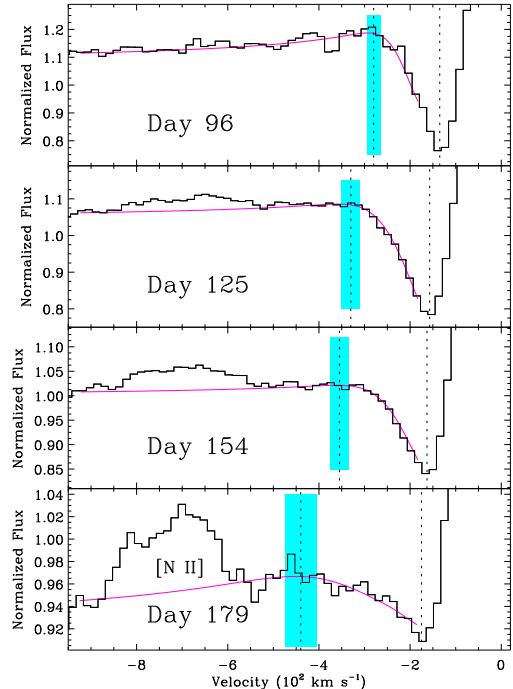


FIG. 15.— Same data as in Figure 14, but zooming in on the narrow $H\alpha$ absorption on each DEIMOS epoch. The purpose here is to show how we defined the blue-edge velocity of the narrow absorption by fitting a smooth curve (magenta) to the transition from the narrow absorption to the blue emission wing, excluding the narrow [N II] $\lambda 6548$ emission. The point where this curve reaches a maximum is taken to be the blue-edge velocity, shown as the vertical dashed line, with uncertainties indicated by the blue box. The velocity of the minimum of the narrow absorption is also marked with a dashed vertical line.

than for a Wolf-Rayet star.

Figure 14 shows the narrow $H\alpha$ absorption and emission feature in SN 2006gy at several epochs as seen in our high-resolution DEIMOS spectra. Two qualitative points are evident from this plot.

(1) The strength of the blueshifted absorption weakens relative to the narrow emission component. On day 96 the two are comparable, implying that it may be a pure scattering P Cygni profile, but as time proceeds, this narrow blueshifted absorption weakens.

(2) The velocities of the absorption minimum and the blue edge of the narrow absorption feature shift to faster speeds at later times. The speeds of the absorption minimum are roughly -135 , -157 , -163 , and -175 (± 5) km s^{-1} on days 96, 125, 154, and 179, respectively. The blue-edge velocities are less clear, but are roughly 280 (± 15), 330 (± 20), 355 (± 20), and 440 (± 35) km s^{-1} on these same days. We define the blue-edge velocity as the point where the intensity turns over and begins to drop down the slope of the broad component, as shown in Figure 15. It is complicated by the presence of [N II] $\lambda 6548$ and by noise or complex structure in the data, so these values are approximate. Nevertheless, it is clear that the velocity changes with time in a systematic way. Kawabata et al. (2009) obtained high-resolution spectra ($R \approx 3600$) on days 127 and 157, and their analysis found that the narrow absorption developed a double component and widened to 690 km s^{-1} . This is not confirmed by our spectra at similar epochs with higher resolution, although we note that we can reproduce a similar in-

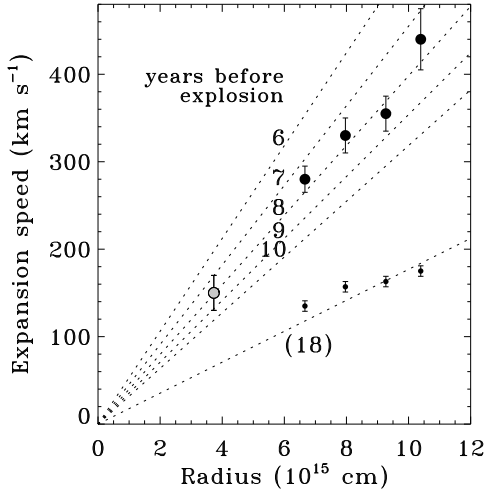


FIG. 16.— Velocities measured from the narrow component of the $H\alpha$ line profile in SN 2006gy on the four DEIMOS epochs in Figure 14, plotted as a function of the presumed forward-shock radius at the same time (see text and Figure 7). The large solid points are the blue edge of the narrow absorption and the small points are the velocity for the absorption minimum. The unfilled point corresponds to the $+150 \text{ km s}^{-1}$ shift of the centroid of the Lorentzian fit to the day 36 $H\alpha$ profile, representing the speed of the CSM outside the shock at that time (see §3.3.1 and Fig. 10). The dashed lines represent the velocity one expects for simple Hubble laws ($V \propto R$) for CSM shell ejection times prior to the SN explosion in years. (The $\sim 18 \text{ yr}$ age that approximates the velocity profile of the absorption minimum is not really representative of the shell age, as the deepest absorption occurs away from the line of sight.)

crease in absorption velocities if we oversubtract neighboring background H II region emission.

The changing depth of the narrow absorption probably results from the simple fact that as the blast-wave radius increases with time and sweeps through the CSM, the total column density of the pre-shock gas is decreasing. This occurs because the immediate pre-shock density should drop with increasing radius, and because increasing amounts of CSM are already swept up behind the shock. This is discussed in more detail in §3.6, in context with the behavior of other narrow absorption lines in the spectrum.

The increasing speed seen in the narrow blueshifted absorption components (Fig. 15) is more interesting, as it directly samples the velocity profile of the pre-SN mass loss. We can use these observed velocities to reconstruct this pre-SN velocity profile and thereby infer the age of the CSM. If we assume that the narrow absorption at each epoch traces cool pre-shock material just outside the forward shock at that time, we can derive its approximate radius away from the progenitor by using the radius given in the bottom panel in Figure 7. (We also assume that the blast wave continues to expand at $\sim 5200 \text{ km s}^{-1}$ after day 110 when the derived value of R_{BB} decreases due to effective optical depth, as explained in §3.2.) Calculating the radius in this way, we plot corresponding values of R and V in Figure 16.

The blue-edge velocities are probably the best indicator of the outflow speed of pre-shock gas along the line of sight at each epoch, whereas the absorption minimum probably traces velocities with some projection from the line of sight closer to the limb of the shell. We see clearly

that the velocity of pre-shock gas along the line of sight increases with radius. We also plot the CSM speed of 150 km s^{-1} inferred from the shifted centroid of the Lorentzian fit to the day 36 $H\alpha$ profile, assuming that it is caused by electron scattering (see §3.3.1). For comparison in Figure 16, we also plot dashed lines corresponding to the velocity profile one expects for simple Hubble laws ($V \propto R$) for CSM shell ejections that occurred 6, 7, 8, 9, and 10 yr prior to the SN explosion. Although the velocities do not perfectly match a linear increasing speed with increasing radius, they are consistent with such a trend within the uncertainties. The age of the CSM shell appears to be $7.8 \pm 1 \text{ yr}$ before explosion, if the expansion has been roughly constant, implying that the massive pre-SN shell ejection experienced by the progenitor of SN 2006gy occurred around October to December 1998.

There are several interesting implications. A Hubble law in the CSM velocity profile means that the observed speeds are *not* the consequence of acceleration of the pre-shock gas by the radiation force of the SN luminosity itself; that mechanism is expected to cause a negative velocity gradient (e.g., Chugai et al. 2002), which is the opposite of the observed trend. Perhaps the pre-shock CSM speeds of other SNe II_n, such as 400, 700, and 1000 km s^{-1} around SNe 1998S, 1995G, and 1994W, respectively (Chugai et al. 2002, 2004; Chugai & Danziger 2003), may reflect their progenitors' ejection speeds, rather than radiative acceleration by the SN.

If the CSM speed really is tied to the physics of the progenitor's mass ejection, rather than having been radiatively accelerated afterward by the SN, it implicates a progenitor object with an escape speed significantly faster than a large RSG, as we discussed in Paper I. Instead, the observed Hubble-like velocity profile points to a relatively sudden episode of mass ejection with speeds of several hundred km s^{-1} . Regardless of the cause, this is similar to the range of velocities and Hubble-like profiles observed in the ejecta of massive LBVs such as η Carinae (Smith 2006a), although the ejecta shell around SN 2006gy was much younger and therefore much closer to the star. In Paper I we noted speculative connections between the precursor event of SN 2006gy and the 1843 eruption of η Carinae based on the H-rich composition, total energy of $\sim 10^{50}$ erg, and ejected mass of order $\sim 10 M_{\odot}$ (Smith et al. 2003), and the ejecta speed. The Hubble-like velocity laws seen in both objects reinforces this comparison. It is also a feature that is explicitly predicted in the model of Woosley et al. (2007), where the pre-SN mass loss is caused by a $\sim 10^{50}$ erg pulsation or explosion triggered by the pair instability. In fact, the observed delay time of 7–9 yr between the precursor and SN 2006gy is in good agreement with the 6.8 yr delay predicted in Woosley et al.'s model. The Hubble-like profile is not consistent with a dense but steady mass-loss wind, indicating that the progenitor star was decidedly unstable leading up to core collapse. For SN 2006gy, the precursor event ejected $\sim 19 M_{\odot}$ at speeds of $200\text{--}500 \text{ km s}^{-1}$, with a corresponding kinetic energy of $\gtrsim 10^{49}$ erg.

The fact that the systematically increasing CSM velocity is seen in absorption means that it corresponds to material along our line of sight. The range of velocities is therefore not likely to be caused by asymmetry

in the CSM, although by no means is this an argument that the CSM is necessarily spherical. We hope to investigate possible effects of asymmetry in a future paper discussing our spectropolarimetry of SN 2006gy. Asymmetry in the CSM is appealing as a potential explanation for the very smooth and slowly evolving light curve (van Marle, Smith, & Owocki 2009b).

3.6. Peculiar Narrow and Broad Absorption Features

Figure 17 gives a detailed view of our high-resolution spectra of SN 2006gy at visual wavelengths from the blue to $H\alpha$, which emphasizes features that make the spectrum of SN 2006gy so distinct. The most remarkable characteristic of the spectrum is the presence of line profiles with both broad and narrow emission and absorption components, leading in some cases to profiles with extremely sharp edges that separate redshifted emission from blueshifted absorption. As we noted earlier in Figure 5, the narrow absorption features in SN 2006gy find their closest comparison with the spectra of SN 1994W and SN 1995G (Sollerman et al. 1998; Chugai & Danziger 2003; Chugai et al. 2004). However, the dual nature of the SN 2006gy profiles — with clearly separate broad and narrow absorption components — was not seen in those two SNe. These lines are not as prominent in any other known SN II_n.

A key point to recognize in Figure 17 is that after first appearing in the day 96 spectrum (and the days 92 and 93 spectra in Figs. 4), the narrowest absorption features become systematically weaker with time. These narrow absorption features at velocities of roughly -200 km s^{-1} are formed in the pre-shock CSM. Their progressive weakening is *not* an effect of increasing or decreasing ionization with time in the pre-shock CSM, since the same trend is seen in narrow absorption of both He I and Fe II lines with widely different ionization state.⁶

This effect signals that the column density of pre-shock absorbing material is probably decreasing with time as the forward shock approaches the outer boundary of a dense shell. The weakening of the narrow absorption features occurs from days 90 to 200; many of the narrow features are barely discernible on day 179. Recall (§3.4.2) that the total line luminosity of $H\alpha$ begins to drop around day 150 and plummets severely by day 209 (Figure 13). The $H\alpha$ emission line is produced primarily in the post-shock gas, which is becoming optically thin at these late phases, so it directly traces the strength of the CSM interaction and hence, the pre-shock CSM density. The fact that both this post-shock $H\alpha$ emission and the pre-shock narrow absorption features weaken at the same time confirms the notion that by day 200, the blast wave of SN 2006gy is overtaking the outer boundary of a shell that was probably ejected ~ 8 yr before core collapse.

Fe II $\lambda 5018$ and $\lambda 5169$: Figure 18 shows the profiles of Fe II $\lambda 5018$ observed at high resolution. This is a strong line that is representative of many other features in the spectrum. The red wing of its smooth broad emission component indicates velocities similar to those of $H\alpha$, suggesting that it is formed in a similar region

of the swept-up CDS. It is not present in the early-time spectrum before and during peak luminosity, when we expect that the photosphere is ahead of the forward shock, but the broad Fe II $\lambda 5018$ emission is present at all times after the post-shock gas becomes optically thin. Figure 18 demonstrates the extremely sharp transition from redshifted emission to blueshifted absorption that is seen in many lines in the spectrum of SN 2006gy. The gray curve in Figure 18 is a symmetric Gaussian matching the red emission wing, showing that Fe II $\lambda 5018$ suffers from significant broad blueshifted self-absorption out to -4000 km s^{-1} , as seen in $H\alpha$. This broad absorption remains constant with time. Fe II $\lambda 5169$ has a similar broad absorption feature, but lacks the broad emission.

Relative to the broad-emission strength, the narrow absorption from the pre-shock CSM weakens with time as noted above for many other lines. Its equivalent width decreases by more than a factor of 2 from day 96 to 179. The velocity of the pre-shock gas causing the narrow Fe II $\lambda 5018$ absorption does not show as clear of an increase with time as had been seen in $H\alpha$, but the day 96 spectrum is noisy for these Fe II lines so it is difficult to evaluate changes in the narrow absorption profile. Fe II $\lambda 5169$ has a narrow absorption feature that is very similar to that of Fe II $\lambda 5018$ (Fig. 18), so we infer that the Fe II $\lambda 5018$ line is not severely affected by possible He I $\lambda 5015$. The narrow Fe II absorption indicates speeds in the CSM of $200\text{--}600 \text{ km s}^{-1}$, consistent with $H\alpha$. The more subtle velocity evolution may suggest that the narrow CSM absorption of Fe II occurs over the full range of radii in the CSM shell, whereas $H\alpha$ absorption occurs preferentially over a smaller range of radii near the blast wave. This could be a result of the more demanding conditions for nebular Balmer absorption as opposed to those needed for Fe II. To fully understand the differences between Fe II and $H\alpha$ absorption and emission, time-dependent radiative transfer models are needed.

Si II $\lambda\lambda 6347, 6371$: Figure 19 shows the profiles of the Si II $\lambda\lambda 6347, 6371$ doublet observed at high resolution. These lines are of particular interest since they are a defining characteristic of SNe Ia, and the presence of this broad absorption feature in spectra of SN 2006gy could suggest a possible connection to objects like SN 2002ic and 2005gj, although as noted elsewhere (Ofek et al. 2007; Paper I), these lines are also seen in some core-collapse SNe.

The Si II $\lambda\lambda 6347, 6371$ doublet exhibits narrow absorption that weakens with time, in agreement with several other absorption lines formed in the pre-shock CSM. The doublet shows no narrow or broad emission components.

More interesting, perhaps, is the broad blueshifted Si II absorption in Figure 19. The shape of the blue wing is compromised by a blend with Fe II, but it is clear that significant broad blueshifted absorption of Si II is present on day 96, out to velocities of roughly -4000 km s^{-1} . This absorption weakens with time, perhaps due to ionization effects, while it is weak or absent in early-time spectra. The speeds traced by this blueshifted Si II are far too slow to arise in a normal SN Ia atmosphere, where speeds well above 10^4 km s^{-1} are seen, but velocities as fast as 4000 km s^{-1} are entirely consistent with speeds we have inferred for the expanding post-shock shell. Similar broad Si II absorption was seen in SN 1998S (Fassia et al. 2001). We conclude that the broad Si II absorp-

⁶ The four narrow Na I absorption lines are in a separate category, as they are formed largely in the Milky Way interstellar medium (ISM) and in the ISM of NGC 1260, rather than in the immediate CSM of the progenitor of SN 2006gy.

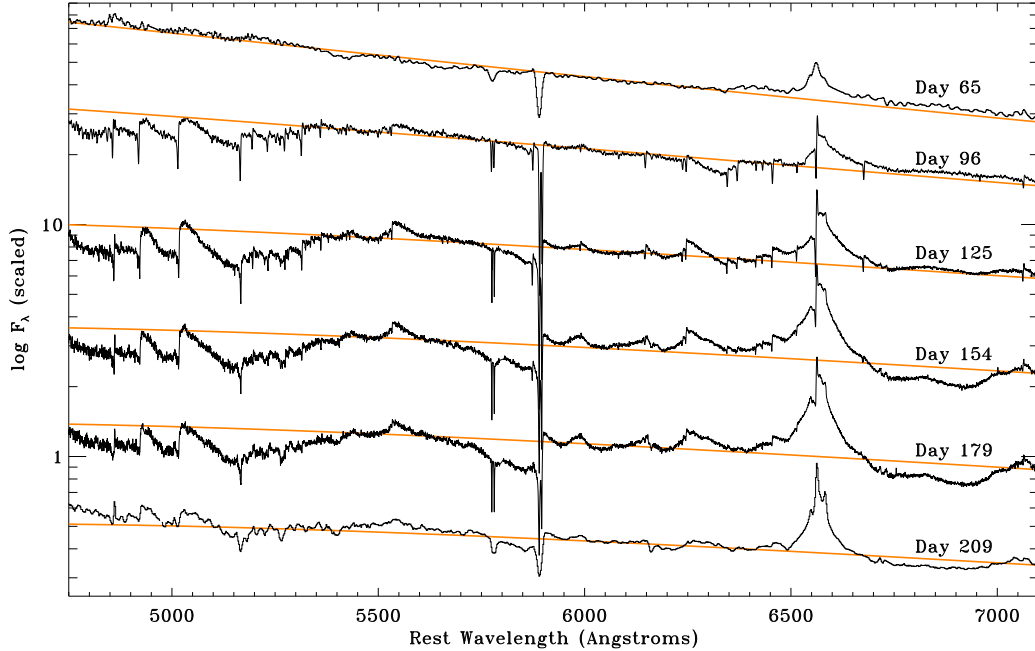


FIG. 17.— Same as Figure 4, but displaying a smaller wavelength range and emphasizing our high-resolution DEIMOS spectra on days 96, 125, 154, and 179, as well as one epoch before and after with lower resolution. These have been dereddened by correcting for both Galactic and host-galaxy extinction as before, with the same underlying blackbodies for comparison (gray; orange in the online edition). A key point is that the many narrow absorption components weaken with time after day 96.

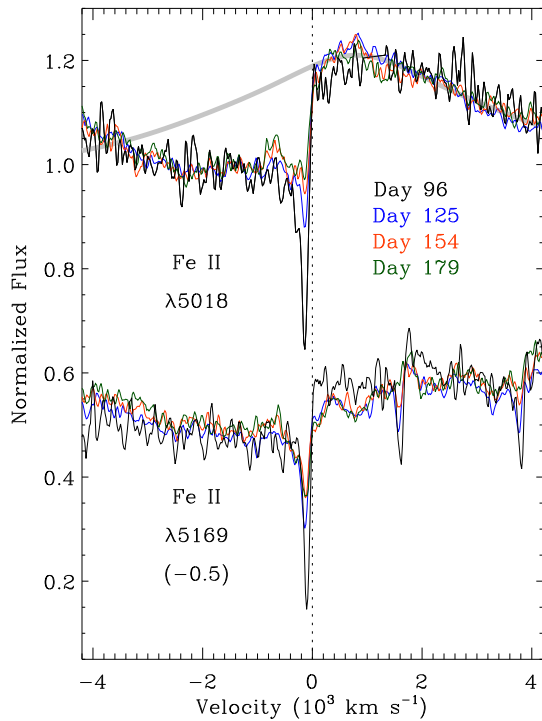


FIG. 18.— The observed profiles of Fe II $\lambda 5018$ in high-resolution DEIMOS spectra. As with $H\alpha$, the narrow absorption becomes relatively weaker with time. The thick grey curve is a 2-component composite Gaussian with the same FWHM velocities as for $H\alpha$, but with different strengths and with its center offset by $+600 \text{ km s}^{-1}$. We also show tracings of Fe II $\lambda 5169$ for comparison.

tion in SN 2006gy is not formed in the photosphere of the underlying SN, but is instead in the post-shock shell, and should therefore not be taken as providing any connection to a putative SN Ia. As noted elsewhere, the post-shock shell is opaque until day 110, so features as-

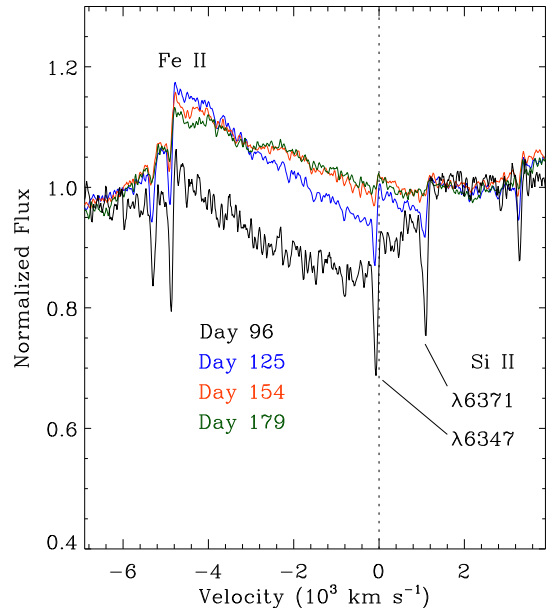


FIG. 19.— DEIMOS spectra at wavelengths surrounding the red Si II doublet, plotted on the velocity scale for Si II $\lambda 6347$. In addition to narrow Si II absorption, possible broad absorption out to a few thousand km s^{-1} is seen on day 96, but its interpretation is complicated because of blending with a Fe II emission feature that strengthens with time.

sociated with the underlying SN photosphere should not be seen before then anyway.

Na I D and He I $\lambda 5876$: The most striking features associated with the Na I line in Figure 20 are the four very narrow absorption features that correspond to the two pairs of Na I absorption lines formed in the Milky Way ISM and in the ISM of NGC 1260. These features do not change much with time when observed at consistent resolution, and support the large values of Milky Way

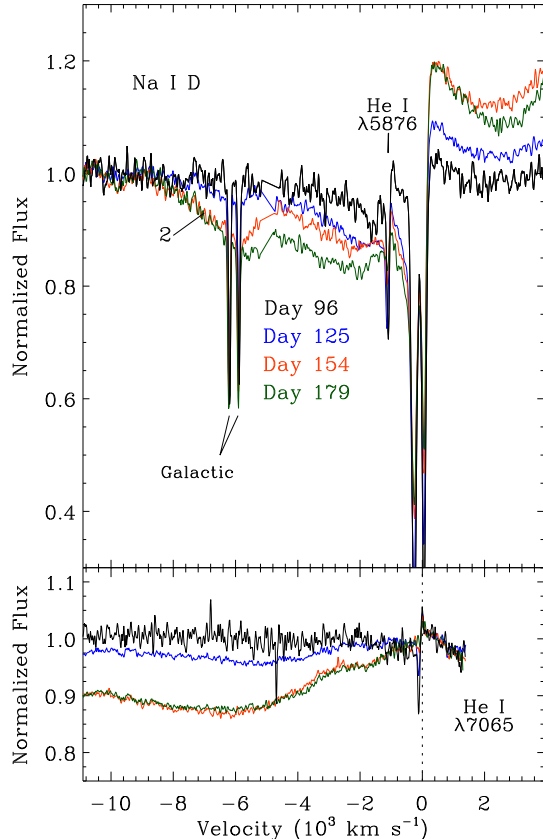


FIG. 20.— *Top*: The observed line profiles near Na I D in high-resolution DEIMOS spectra, including broad emission and absorption of Na I (or He I), Galactic and host-galaxy narrow absorption from Na I, plus weak narrow absorption and emission from He I $\lambda 5876$. *Bottom*: Tracings of He I $\lambda 7065$ in the same data for comparison.

and host-galaxy reddening that we inferred in Paper I. Figure 20 also reveals narrow absorption and emission from He I $\lambda 5876$ (and $\lambda 7065$), consistent with other narrow He I features in the spectrum.

The identification of the broad emission in the top panel of Figure 20 is unclear. Due to the proximity in wavelength of Na I D and He I $\lambda 5876$, it could be either or both at different times. It follows the same trend of increasing equivalent width of H α emission over the same time period. Since Na I is expected to be strong under similar conditions in SN II spectra (e.g., Dessart & Hillier 2008) and because similar increases in strength are not seen in emission components of other He I lines (like He I $\lambda 7065$; bottom of Fig. 20), we surmise that the broad *emission* component is Na I.

The nature of the broad *absorption* in Figure 20 is more perplexing. This absorption strengthens with time, whereas Fe II $\lambda 5018$ stays roughly constant and Si II decreases in strength with time. Unlike any broad absorption features discussed so far, it reaches to velocities as fast as -8000 km s^{-1} on days 154 and 179. The broad absorption blueward of He I $\lambda 7065$ behaves very differently in velocity and time (Fig. 20, bottom), so we conjecture that *both* features cannot be He I absorption; perhaps neither are.

The higher-speed absorption near Na I may be due to a second absorbing species that we refer to here as component 2 (see Figure 20). The relative contribution of

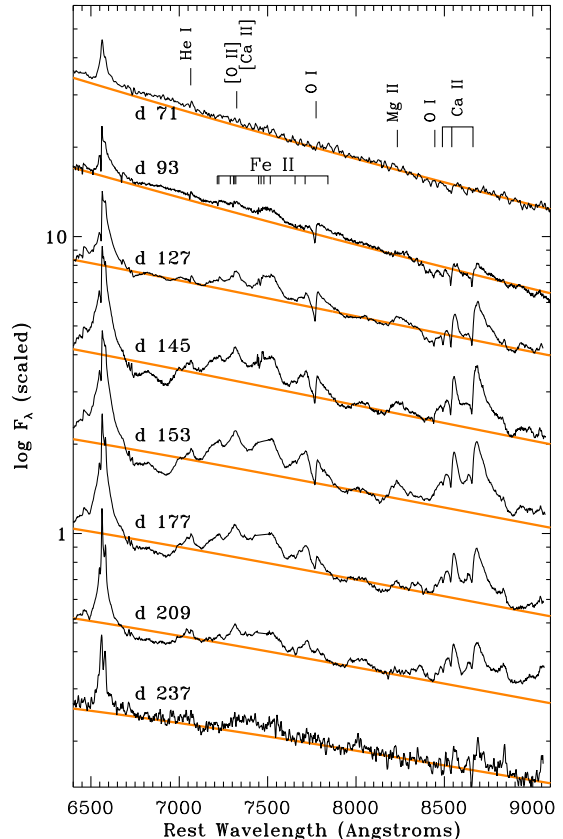


FIG. 21.— LRIS spectra at red wavelengths, plus one Lick/Kast spectrum at peak luminosity for comparison. Several line identifications are marked (see Dessart et al. 2009). Representative blackbodies are shown (gray; orange in the online edition) as in Figure 4.

component 2 changes with time; it is initially absent and then becomes prominent on days 154 and 179, forming an additional dip at velocities of -5000 to -8000 km s^{-1} that was absent before day 154. It seems likely that this additional absorption is due to a superposed line of another species, since (a) the strength of component 2 changes differently from the rest of the broad absorption feature, (b) it is not seen in any other broad absorption line, and (c) fast SN ejecta with speeds of $\sim 8000 \text{ km s}^{-1}$ should have already caught up with the reverse shock by day 80 (see §4.3). It may, however, be related to other broad absorption features at red wavelengths that strengthen at the same time, like the broad absorption blueward of He I $\lambda 7065$.

3.7. LRIS Spectra at Red Wavelengths

We obtained six epochs of high signal-to-noise ratio (S/N) spectra with LRIS on Keck (plus a last epoch on day 237 with lower S/N; see Table 1). These are particularly useful for investigating the evolution of the red-wavelength spectrum of SN 2006gy (Fig. 21), not sampled by our high-resolution DEIMOS data. The day 71 spectrum is included in Figure 21, representative of our three early epochs of Lick/Kast spectra on days 36, 65, and 71, which exhibit essentially featureless blackbody continua at red wavelengths with perhaps some weak absorption in the Ca II near-IR triplet and weak emission of He I $\lambda 7065$.

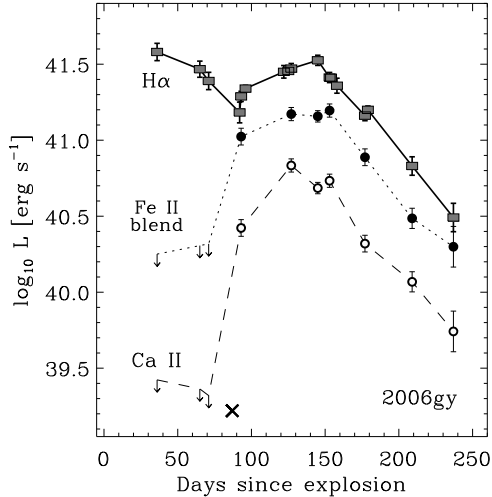


FIG. 22.— The luminosity of the $H\alpha$ line from Figure 13 is compared with the integrated luminosities of the red Fe II blend over roughly 7130–7620 Å (filled circles) and that of Ca II $\lambda 8662$ (unfilled circles). The first three points for both Fe II and Ca II are generous upper limits; these features are not seen in the spectrum at early times. The “X” marks the soft X-ray luminosity of SN 2006gy detected by *Chandra* that we reported in Paper I.

As shown by our sequence of LRIS spectra in Figure 21, the post-maximum red-wavelength spectrum evolves with time. Prominent emission features are He I $\lambda 7065$, a blend of several Fe II emission lines, O I $\lambda 7774$, and the Ca II near-IR triplet. The last of these is particularly interesting; it becomes nearly as strong as $H\alpha$, suggesting that it may be a significant source of post-shock cooling in SNe II_n. A possible blend of [O II] and [Ca II] near 7325 Å also appears to be present, although we cannot be confident of the identification of these forbidden lines because they overlap with several Fe II lines. The spectra in Figure 21 are roughly consistent with previous reports, but have better temporal sampling and wavelength coverage. Agnoletto et al. (2009) noted that the Ca II triplet was present in their spectrum on day 174; our spectra show that this was after the time when this line was strongest and was already in a steady decline. Spectra on days 127 and 157 presented by Kawabata et al. (2009) showed He I $\lambda 7065$ and a few of the Fe II emission lines out to ~ 7400 Å, although in our spectra near those dates, these features appear stronger relative to the continuum. Lines in our red spectra during days 100–240 do not correspond well with those in later spectra on day 394 identified by Kawabata et al. (2009).

Our spectra reveal that the flux of these features changes notably with time. In Figure 22 we compare the temporal evolution of the integrated luminosity of the Fe II blend and that of Ca II $\lambda 8662$ with the $H\alpha$ luminosity (from Figure 13). To represent the behavior of the Fe II blend while avoiding the strong O I $\lambda 7774$ absorption, we took the flux above the continuum as it appears in Figure 21 measured over ~ 7130 –7620 Å. For Ca II $\lambda 8662$, we measured the line strength integrating over roughly $-2,000$ to $+4,000$ km s⁻¹. These emission features are not seen in early-time spectra, so for those epochs we give conservative upper limits.

Figure 22 shows a very interesting trend. The Fe II and

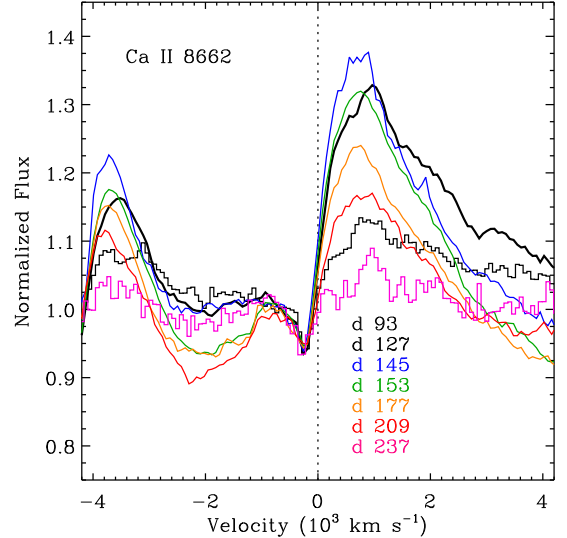


FIG. 23.— LRIS spectra of Ca II $\lambda 8662$ at several epochs. These have been arbitrarily normalized at the minimum of the narrow absorption. The first two phases we plot, shown in black, are while the line luminosity is increasing with time on days 93 (thin black histogram) and 127 (thicker black line). After reaching its peak luminosity on day 145 (blue), the Ca II $\lambda 8662$ line weakens systematically with time (blue, green, orange, red, and magenta on days 145, 153, 179, 209, and 237 respectively).

Ca II emission track the behavior of the $H\alpha$ luminosity almost exactly after day 90, but at earlier times they are relatively much fainter than $H\alpha$. The likely implication is that the Fe II lines and the Ca II triplet trace emission directly from the post-shock cooling shell that is the product of CSM interaction, which is invisible at early phases because it is behind the external photosphere. The same is true for the intermediate-width $H\alpha$ in post-maximum phases. At early times, however, when the post-shock $H\alpha$ is hidden behind the photosphere, the emergent $H\alpha$ line is dominated by a completely different emission mechanism. As we proposed above, the intermediate-width $H\alpha$ emission at early times probably arises from photoionized pre-shock circumstellar gas and subsequent scattering by thermal electrons. We find, therefore, that red Fe II lines and the Ca II triplet are more robust tracers of the direct CSM interaction luminosity than $H\alpha$, since intermediate width $H\alpha$ can be produced by a different mechanism. The Ca II lines have no narrow emission at any epoch.

The red Fe II lines are too blended to derive individual line-profile shapes, but the profile of Ca II $\lambda 8662$ is displayed in Figure 23 as seen in all our epochs of LRIS spectra. Like $H\alpha$, Ca II $\lambda 8662$ has a bright intermediate-width emission component with a half-width of roughly 2,000 km s⁻¹ and broader line wings. Although the strength of the line changes, its width does not change much. Ca II $\lambda 8662$ also has a sharp narrow blueshifted absorption component at roughly -200 km s⁻¹, and is missing the blue side of the line, suggesting rather strong broad blueshifted absorption. Based on the similarity of their red emission wings, $H\alpha$ and Ca II probably trace similar regions in the dense shell.

The presence of strong intermediate-width lines of Ca II from the post-shock gas is of potential interest with regard to SN 2008S and the similar transient in NGC 300, both of which showed particularly strong emission of $H\alpha$, [Ca II], and the Ca II near-IR triplet (Smith et al. 2009b);

Bond et al. 2009; Berger et al. 2009). SN 2006gy also may show the [Ca II] lines, although we cannot reliably separate them from [O II] and Fe II lines.

Lastly, we note the presence of broad absorption features at 6700–7000 Å, where the red wing of H α meets the continuum. Signs of this absorption first appear on day 127, and the absorption strengthens with time on days 145 and 153. It subsides at subsequent epochs and disappears by day 237. The change in strength of the broad absorption features follows, in rough relative terms, the strength of the emission in the red Fe II and Ca II lines noted above. Prominent absorption at these wavelengths appears to be a common feature in late-time spectra of luminous SNe IIn such as SNe 1997cy, 1999E, 2002ic, and 2005gj. For example, the day 98 spectrum of SN 2005gj is shown in Figure 5; it exhibits a single very broad and prominent absorption feature at these wavelengths. In SN 2006gy this feature is either composed of two separate species with absorption minima at \sim 6750 and 6930 Å, or alternatively, the two parts are separated by a superposed emission feature at 6820 Å.⁷

The identification of these broad absorption lines is uncertain. Broad lines near the wavelengths of these features are seen in SN photospheres of Types Ia, Ib, and Ic at late times, although the different expansion speeds make a direct comparison with SN 2006gy difficult. This feature was part of the rationale for associating SNe 2002ic and 2005gj with SNe Ia, although Benetti et al. (2006) have questioned this association and suggested SNe Ic as the culprit instead. SN 2006gy informs this debate for the following reason: *In the case of SN 2006gy, these absorptions cannot be due to features in an underlying SN photosphere, because they are too strong.*

The fact that features are seen in absorption at such late phases requires the presence of some substantial source of background continuum light. At its strongest, the broad absorption reaches a depth of roughly 12–15% of the continuum level (Fig. 22), requiring that the underlying source that is being absorbed has a luminosity of $(1\text{--}2) \times 10^9 L_{\odot}$ at the late phases of 120–170 days when this absorption is seen. No standard SN photosphere is that luminous at such late times, so these lines cannot arise in a simple scenario of normal SN ejecta being seen through the thinning CSM interaction region. The luminosity may come from the reverse shock or radioactive decay, as we discuss further in §4.1. More complicated effects may play a role as well, such as “top-lighting” (e.g., Branch et al. 2000), caused by irradiation of the SN ejecta by photons emitted from the CSM interaction region. Since SNe with strong CSM interaction like SN 2006gy can mimic features seen in other SNe, this casts doubt on the association of such features with an underlying SN Ia photosphere in other luminous SNe IIn. This would seem to support claims by Benetti et al. (2006) that this class of objects could be SNe other than Type Ia.

Regardless of the identification, from the broad line profiles and the fact that they do not appear until late times, it is likely that these lines arise from SN ejecta that

have just crossed or are just about to cross the reverse shock. As we note below, the speeds of unshocked SN ejecta and the expansion speed of the CDS in the post-shock gas are comparable at these late times.

4. DISCUSSION

4.1. SN 2006gy Spectral Evolution Overview

Altogether, the extraordinary spectral properties of SN 2006gy can be understood in the context of CSM interaction where the radiating layers evolved through three key phases in the first year, as follows.

(1) *Early times (days 0–90)*: At these phases before and up to the time of maximum luminosity, the photosphere is outside the forward shock and the spectrum is generated in the pre-shock CSM. Radiation diffusing from the shocked shell propagates forward and pre-ionizes the opaque CSM, leading to a smooth continuum plus Balmer lines generated in CSM layers immediately outside that. Consequently, the post-shock CDS and the SN ejecta cannot be seen yet. The intermediate-width H α line profile arises because narrow lines from the photoionized pre-shock CSM are broadened by multiple scattering with thermal electrons in the opaque gas (e.g., Chugai 2001). This hypothesis is consistent with the observed H α /H β intensity ratio indicative of recombination at early times, and the Lorentzian profiles of H α line wings. At this phase, therefore, the prime luminosity source is diffusion of shock-deposited energy (Smith & McCray 2007) in a manner similar to that described by Falk & Arnett (1977).

(2) *Decline from Maximum Luminosity (days 90–150)*: During these phases, the photosphere recedes (in mass) past the forward shock and into the CDS. As the photosphere passes this sharp boundary, the consequent transition in spectral morphology from phase 1 to phase 2 may be sudden. The effective value of R_{BB} begins to fall, not because the radius is actually decreasing, but because the CDS is fragmented and is becoming progressively more transparent (Smith et al. 2008a). As the CDS is exposed, we begin to see strong emission from cooling lines in the post-shock regions, such as multiple Fe II and Ca II lines, which turn on suddenly after day 90, in addition to broad H α . Broad blueshifted absorption features (see §4.2 below) appear during this time as the photosphere is now inside the CDS, and outer layers of the CDS can be seen in absorption. The broad emission-line wings and the blueshifted absorption show that the expansion velocity of the CDS does not slow during this time period, indicating self-similar expansion. The broad line-wing shape is probably a composite of the true kinetic line width (about 4000 km s⁻¹ as indicated by the blueshifted absorption) plus a contribution from electron scattering within the clumpy CDS itself (not in dense CSM as in stage 1; see Dessart et al. 2009).

Much of the continuum luminosity during this time is still supplied by fading diffusion from the gradually thinning shocked shell, possibly reheated from within by reverse-shock luminosity, but there is also a significant contribution now from ongoing CSM interaction luminosity. The continuum effective temperature remains roughly constant. The speed of the pre-shock CSM appears to be increasing during this time, suggesting a Hubble-like flow in the episodic pre-SN mass loss that

⁷ Note that SN 2005gj exhibits an even stronger and broader absorption feature at \sim 8000 Å that is not seen in a comparable way in SN 2006gy at any epoch. It is therefore possible that the 6700–7000 Å broad absorption features in SNe 2005gj and 2006gy are unrelated.

occurred ~ 8 yr before explosion. In addition, there is suggestive evidence that during this phase we also see some broad absorption features from the underlying SN ejecta that are about to cross or have just crossed the reverse shock. If true, the interesting implication is that this absorption requires a fairly substantial *background* continuum luminosity source of $\sim 10^9 L_{\odot}$.

(3) *Drop in Late-Time CSM Interaction (days 150–240)*: Beginning around day 150, diagnostics of the post-shock cooling luminosity, such as $H\alpha$, Fe II, and Ca II lines (see Figure 22), show a precipitous and continuing decline. At these late phases the emitting layers must be optically thin and getting thinner with time, so the weakness of these lines cannot be attributed to high optical depth as before. Instead, the decline probably indicates that the CSM interaction luminosity itself is dropping as the forward shock reaches the outer boundary of the dense pre-SN shell ejected 8 yr earlier. A key point is that during the transition from stage 2 to stage 3, the narrow absorption components formed in the pre-shock CSM were observed to weaken and disappear in some cases, signaling lower pre-shock densities upstream, and heralding the inevitable approach of the outer boundary of the dense pre-shock CSM. This confirms that the reason the $H\alpha$, Fe II, and Ca II line luminosities dropped at late times was because the SN ran out of CSM to sweep up, not because the SN ran out of energy or recombined.

The drop in CSM interaction at days 150–240 explains why the late-time spectrum observed 1 yr later showed no sign of ongoing CSM interaction. $H\alpha$ was observed to be about 400 times weaker than in SN 1988Z or SN 2006tf at a comparable epoch (Smith et al. 2008b).

Returning to the spectral behavior during stage 3 at days 150–240, then, it remains quite perplexing why the continuum luminosity did not drop by an amount comparable to the drop in $H\alpha$, Fe II, and Ca II as it did in SN 1994W (Chugai et al. 2004). *It should have dropped if it were generated primarily by CSM interaction.* Instead, the red-continuum luminosity appears to have slowed its decline during this stage and even seemed to level off at late times. The SN was still quite bright at these late times — it was still as luminous as the peak of a normal Type Ia — so this extra late-time luminosity source after day 200 is nontrivial.

Given the difficulty imposed by the proximity of the host-galaxy nucleus, it is conceivable that some of the blue-wavelength light after day 200 is contaminated by host-galaxy light, but red wavelengths show a clear detection of the SN. In a companion paper (Miller et al. 2009b), we confirm that the lingering emission detected 1–2 yr later is indeed due to a light echo as proposed by Smith et al. (2008b). However, a reflected-light echo is not a satisfying explanation for the extra luminosity around days 200–240, because (1) the continuum shape observed then was redder than that at the time of peak luminosity; we would expect reflected light to be the same as or bluer than the original spectrum, as it is at later times (Miller et al. 2009b), and (2) a distant light echo cannot give rise to the broad absorption features seen in the spectrum (§3.7).

One possibility for the excess emission at days 200–240 is a re-energized reverse shock, powered by increased density of SN ejecta crossing the reverse shock and re-heating the CDS from the inside. Even if the CSM density drops

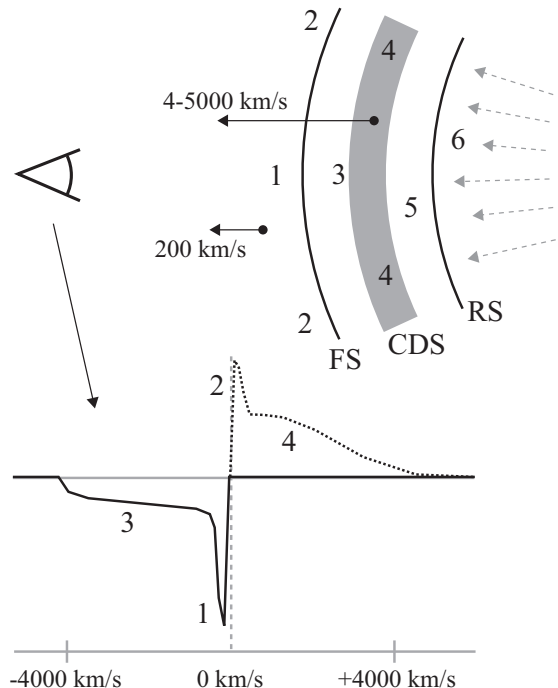


FIG. 24.— Sketch of the emitting geometry in SN 2006gy that leads to the formation of its unusual spectral line profiles. FS, RS, and CDS refer to the forward shock, reverse shock, and cold dense shell, respectively. Narrow absorption (1) occurs in the pre-shock gas near our line of sight, while narrow emission (2) occurs in other parts of the ionized pre-shock gas. The broad emission component (4) is emitted by cooling gas in the CDS, while the broad blueshifted absorption (3) occurs somewhere between the FS and the continuum photosphere that is within or behind the CDS. The relative strength of components 1, 2, 3, and 4 in a spectral line depends on the ionization level of the observed species, its relative abundance, and the temperature and density of the gas where it is emitted, so not all line profiles look the same. Many overlapping profiles produce the peculiar shape of the spectrum of SN 2006gy. At late times when the CDS begins to fragment and becomes optically thin (after day ~ 115), we may start to see broad emission features from swept-up ejecta (5) or the freely expanding ejecta (6).

so that the forward shock no longer encounters a significant obstacle, the massive CDS that has already formed and is now coasting at 4000 km s^{-1} provides a wall that may decelerate the faster SN ejecta passing the reverse shock. Alternatively, some of the extra luminosity of $(1-2) \times 10^6 L_{\odot}$ needed for the broad absorption features seen on days 120–170 could be supplied, hypothetically, by radioactive ^{56}Co decay from $\lesssim 2.5 M_{\odot}$ of ^{56}Ni . Unfortunately, SN 2006gy was aligned too closely with the Sun after day 240 and we were no longer able to observe it until the later data reported by Smith et al. (2008b), when it had already faded considerably. See Miller et al. (2009) for additional discussion of the late-time data.

4.2. Origin of the Composite Line Profiles: CSM Interaction Seen in Absorption

Here we take a more detailed and qualitative look at the origin of the unusual spectrum of SN 2006gy during the second stage described above, days 90–200 when it showed several overlapping complex, peculiar line profiles. While SN 1994W and SN 1995G showed similar spectral lines at earlier epochs, with narrow emission and absorption, they did not exhibit such prominent broad absorption features that give SN 2006gy its distinct spec-

tral appearance.

A cartoon of a hypothetical line profile for a single line is shown in Figure 24. The narrow and broad absorption (components 1 and 3, respectively) are common to many lines in the spectrum. The narrow and broad emission, components 2 and 4, are seen in some lines and not in others, depending on the ionization state, temperature, and density of the gas. For example, (a) both emission components are absent in the red Si II doublet, (b) only the broad emission is present in Fe II $\lambda 5018$ and Ca II $\lambda 8622$, and (c) both narrow and broad emission are seen in H α . One can imagine that a series of these line profiles seen in superposition, having different strengths of absorption, with or without either emission component, can lead to the high-resolution spectrum of SN 2006gy seen in Figure 17. Whether self-consistent radiative transfer calculations can account for the appearance of the spectrum is a more difficult challenge.

Figure 24 also indicates the likely places where components 1, 2, 3, and 4 may be produced in a simplified CSM-interaction scenario (by “simplified”, we mean that we do not show the clumping, instabilities in the CDS, or large-scale asymmetry that are all possible). Because of their low velocities, the narrow components 1 and 2 must arise in the pre-shock CSM, either in absorption along our line of sight (1) or in emission away from our direct line of sight (2). Such narrow features are common in spectra of SNe II_n with sufficient resolution.

The broad (actually intermediate-width) emission component (4), which is a common characteristic of SNe II_n, is formed in the CDS expanding at ~ 4000 km s⁻¹ during this time interval (days 90–200). We showed that the intermediate-width H α emission component can be approximated as a symmetric composite Gaussian with two components of roughly equal intensity, one with FWHM = 5200 km s⁻¹ and one with FWHM = 1800 km s⁻¹. While these distinct velocities are somewhat artificial, this emission component likely arises as a result of the intrinsic kinematic line profile plus broadening of the line wings due to electron scattering within the optically thick CDS itself. Note that electron scattering within the line-forming region in the CDS, as suggested by Dessart et al. (2009), is different from the electron scattering that broadens the wings of narrow lines formed in the CSM that we discussed earlier (§3.3.1; see Chugai 2001). We suspect that both are at work in SN 2006gy at different times — one in the early-time spectra when the photosphere was outside the shock, and one during the decline from peak luminosity when the photosphere and H α -emitting region were in the CDS. The idea that electron scattering plays a role in forming the broad wings of H α is supported by the fact that they are unchanging with time, and that the blue H α emission wing extends to faster speeds (5000–6000 km s⁻¹) than the blue edge of the blueshifted H α absorption at 4000 km s⁻¹. Different lines, like Fe II and Ca II, originate from different optical depths within the CDS and will therefore be modified to differing degrees by electron scattering. Whether different line-profile shapes are consistent with this hypothesis is another challenge for detailed calculations. Dessart et al. (2009) have shown, for example, that even different H I lines have different line wings for this reason.

The broad blueshifted absorption in SN 2006gy (com-

ponent 3) is unusual among SNe II_n because most exhibit symmetric wings of the intermediate-width H α line, sometimes even showing enhanced blueshifted emission because the back side of the SN is blocked by the optically thick CDS. The dramatic difference in blueshifted H α wings of SN 2006gy and SN 2006tf is shown in Figure 7 of Smith et al. (2008a). While many SNe II_n do show blueshifted absorption, it is usually from narrower components formed in the CSM. The absorption in component 3 of the SN 2006gy line profiles is far too broad to arise in the CSM, and must therefore reside between the FS and the photosphere. The most likely location is in outer layers of the CDS, as long as the continuum photosphere is in deeper layers. The source of the continuum could, in principle, be a combination of background light from the underlying SN ejecta or continuum generated in deeper layers of the CDS which absorb X-rays generated in the reverse shock. This last scenario requires that the SN ejecta of SN 2006gy can still be an important source of kinetic energy, even at late times.

4.3. A Simplified CSM-Interaction Model

Figure 25 summarizes several physical aspects of SN 2006gy interpreted in the format of a standard CSM-interaction model. This is not a hydrodynamic model, but rather a set of parameters derived from observations with a few simplifying assumptions. Two key observed values are the SN’s bolometric luminosity and the radius of the CDS which emits the intermediate-width H α line. The solid circles in Figures 25a and 25b are just the bolometric luminosity and R_{BB} from Figure 7, while the solid black curves are simple continuous approximations of the data. We assume that the true shock radius R continues to increase at roughly constant speed even though the apparent R_{BB} begins to decrease around day 115. The rationale for this is explained in §3.2. Gray lines in Figure 25b represent trajectories for unperturbed SN ejecta.

Figure 25c shows three relevant expansion speeds. At each time t , the speed of the fastest freely expanding SN ejecta that are reaching the radius of the reverse shock (assumed to be the same as R) is simply $V_{\text{ejecta}} = R/t$, shown by the dotted curve. The speed of the CDS, V_{CDS} , plotted in Figure 25 is just the instantaneous value of R . For our purposes here, we assume the post-shock cooling zone in this radiative shock to be very thin, so that $R \approx R_{\text{FS}} \approx R_{\text{RS}}$. The solid line representing V_{CDS} in Figure 25c is consistent with the relatively constant observed speeds of 4000–5000 km s⁻¹ seen in H α from the time of peak luminosity onward. Also, these values of V_{ejecta} and V_{CDS} are consistent, at least qualitatively, with expectations of hydrodynamic models of SNe II_n (e.g., Chugai & Danziger 2003). The dashed line in Figure 25c is the approximate speed of the progenitor’s wind or CSM shell, V_{CSM} , that is being overtaken by the blast wave (V_{CSM} is multiplied by 10 for display). This is inferred from observations of the blue edge of the narrow absorption component of H α , shown in Figure 14. One exception is that we have set the minimum speed at small radii to 150 km s⁻¹; this assumption is irrelevant except for the role that V_{CSM} plays in deriving \dot{M} below.

To calculate the remaining parameters in Figure 25d, we adopt the standard equation for the maximum lumi-

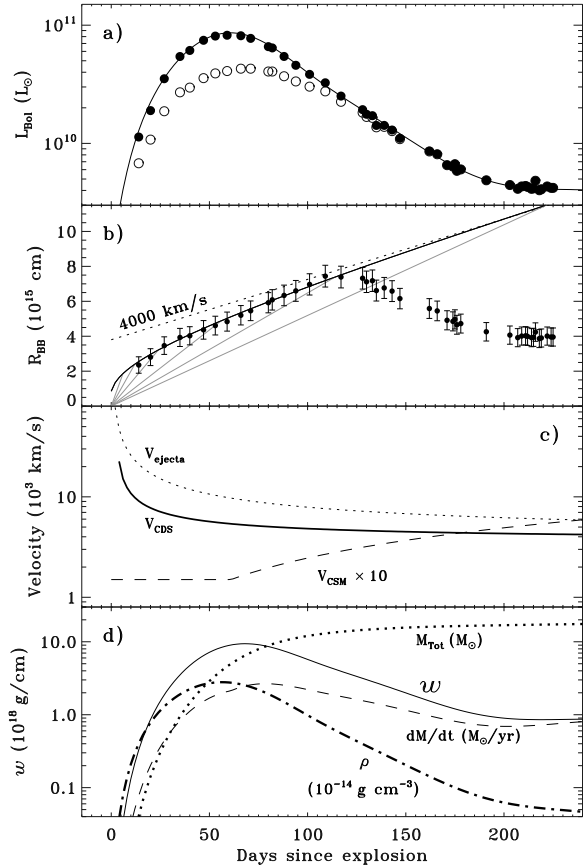


FIG. 25.— A model of the basic parameters of SN 2006gy derived from observations in a simplified CSM-interaction formalism. (a) and (b) are the observed luminosity and radius, respectively, from Figure 7. The smoothed curves in both panels are used to represent the observed bolometric luminosity and radius of the shock, which are needed to derive many other parameters below. In panel (b), the true shock radius continues to increase as R_{BB} , as described in the text. The dashed line shows constant-speed expansion at 4,000 km s^{-1} for comparison, while the gray lines show trajectories for unperturbed SN ejecta in free expansion at 35, 20, 15, 10, 7.5, and $6 \times 10^3 \text{ km s}^{-1}$. (c) The corresponding expansion speeds of the cold dense shell, V_{CDS} , and the SN ejecta that are crossing the reverse shock, V_{ejecta} , as a function of time. Values at $t < 10$ days are poorly constrained. The dashed line is the assumed speed of the progenitor’s wind or CSM shell, V_{CSM} . This is taken from Figure 14, except that we have set the minimum speed at small radii to 150 km s^{-1} ; this assumption is irrelevant except for deriving \dot{M} below. (If we had allowed V_{CSM} to continue to decline at small radii, then the derived value of \dot{M} before day 70 would be smaller.) (d) Plotted values are the instantaneous values one would derive for the wind density parameter, w , the progenitor’s mass-loss rate, dM/dt , the CSM density, ρ , and the cumulative value of the total CSM mass swept up by the shock. Assumptions for deriving these values are explained in the text.

nosity that can be generated by CSM interaction, assuming 100% efficiency, given by

$$L = \frac{1}{2} w V_{CDS}^3, \quad (1)$$

where w is the wind density parameter $w = 4\pi R^2 \rho$, or $w = \dot{M}/V_{CSM}$, and V_{CDS} is the value for the evolving speed of the CDS derived from \dot{R} above. The efficiency may be substantially less than 100% (a value of 30–50% is probably more realistic), which would act to *raise* all the derived values plotted in Figure 25d. The wind density

parameter is plotted here in units of $10^{18} \text{ g cm}^{-1}$ (this is quite a large fiducial value, even for luminous SNe II_n). The true wind density is $\rho = w/4\pi R^2$, plotted here in units of $10^{-14} \text{ g cm}^{-3}$, and the mass-loss rate of the progenitor star inferred at a given time is $\dot{M} = w V_{CSM}$. The value of M_{Tot} given by the dotted line is the cumulative CSM mass that has been swept up by the shock and now resides in the CDS.

A key assumption here is that direct radiative cooling from the post-shock gas supplies the observed instantaneous value of the luminosity. We have argued elsewhere that this is problematic on observational grounds (Paper I) because of the weakness of $H\alpha$ and X-ray emission compared to the continuum, and have suggested that some of the peak luminosity may in fact be due to the delayed escape or diffusion of shock-deposited thermal energy from earlier CSM interaction. If true, the net result is that the values of w , ρ , and \dot{M} in Figure 25d will be overestimated around the time of peak luminosity, but severely underestimated before then.

We see from Figure 25 that the swept-up mass needed to provide the luminosity of SN 2006gy in a CSM-interaction scenario is already $10 M_{\odot}$ (or perhaps 2–3 times more if the efficiency in converting kinetic energy to visual light is not 100%) by the time of peak luminosity, and almost $20 M_{\odot}$ by 200 days after explosion. This large mass dictates that the dense shell must have very high optical depths and a long diffusion time. The $\sim 10 M_{\odot}$ swept up by the time of peak luminosity matches the value adopted by Smith & McCray (2007) in such a model. It is therefore likely that the low CSM density before day 50 (i.e. at $R \lesssim 4 \times 10^{15} \text{ cm}$) plotted in Figure 25d is erroneous, since it stems from the probably false assumption (at early times) that the observed luminosity directly traces CSM-interaction. In reality, high optical depths prevent the shock-deposited thermal energy from escaping promptly, leading to a value from Eq. (1) that is too low.

The need for higher densities at inner radii (within $4 \times 10^{15} \text{ cm}$) is evident from a separate line of reasoning as well. The spectrum at early times (e.g., day 36) arises because the photosphere is outside the forward shock, since shock luminosity must diffuse out through the opaque CSM shell. In the process, multiple scattering with thermal electrons broadens the narrow $H\alpha$ emission from the photoionized pre-shock gas, causing the symmetric profiles. This picture, however, necessitates pre-shock CSM density on day 36 exceeding that on days 90–100 when the pre-shock CSM is no longer opaque. On day 36 we found an optical depth for the pre-shock CSM of roughly $\tau \approx 15$, whereas on days 90–100 it must have been $\lesssim 1$ because the CDS is seen. The inferred CSM densities for days 36 and 90 in Figure 25d, however, are comparable, which cannot be the case. This discrepancy can be reconciled if we relax the assumption that the observed luminosity traces the level of CSM interaction, and is instead due to delayed diffusion at early times. Much higher CSM densities, probably above $10^{-13} \text{ g cm}^{-3}$, are required at inner radii of $2 \times 10^{15} \text{ cm}$. Indeed, CSM densities of 10^{-13} to $10^{-12} \text{ g cm}^{-3}$ were required at these inner radii in models of SN 1994W by Chugai et al. (2004), which showed qualitatively similar spectral properties although at lower luminosity. SN 2006gy probably requires

even higher densities at these inner radii.

In any case, by late times (200–250 days after explosion,) the total CSM mass that has been swept up into the CDS by the shock is 18–19 M_{\odot} . This agrees with the value predicted in the models of Woosley et al. (2007) for a pulsational pair-instability ejection. With a final coasting velocity of $\sim 4000 \text{ km s}^{-1}$, the kinetic energy remaining in the CDS when the strongest CSM-interaction phase has ended is then at least $(2.9\text{--}3.0) \times 10^{51} \text{ erg}$ (it may be considerably more if significant mass is added by the SN ejecta entering the reverse shock). Combined with the integrated radiated energy of $E_{rad} = (2.3\text{--}2.5) \times 10^{51} \text{ erg}$ (§3.2), the initial kinetic energy of SN 2006gy was more than $5 \times 10^{51} \text{ erg}$ and the efficiency in converting energy into visual light was $< 50\%$. This efficiency, in turn, suggests SN ejecta that were at least as massive as the swept-up CSM, implicating a very massive progenitor star.

Qualitatively, the CSM-interaction scenario we suggest for SN 2006gy is actually quite analogous to scaled-up models proposed for SN 1994W and SN 1995G by Chugai et al. (2004) and Chugai & Danziger (2003), respectively. In both cases, the authors proposed that the observed luminosity was due to a combination of internal energy leakage from an extended pre-SN shell, plus subsequent luminosity from CSM interaction. This is qualitatively identical to our proposed model for SN 2006gy, where the prime luminosity source at early times is the slow diffusion of shock-deposited energy in an unbound opaque CSM envelope ejected ~ 8 yr before the SN (see Smith & McCray 2007), and data at late times show an increased contribution from the post-shock shell. In the case of SN 1994W the pre-SN shell was ejected 1.5 yr before explosion in a $2 \times 10^{48} \text{ erg}$ event (Chugai et al. 2004), and for SN 1995G it was ejected 8 yr before in a $6 \times 10^{48} \text{ erg}$ event (Chugai & Danziger 2003). This is reminiscent of the SN 2006gy pre-SN outburst, which occurred ~ 8 yr before with $\gtrsim 10^{49} \text{ erg}$. Both SN 1994W and SN 2006gy showed clear evidence that the strength of CSM interaction plummeted as the blast wave overtook the outer boundary of this CSM shell.

The primary difference between SN 2006gy and the other two events is that, quantitatively, SN 2006gy is a much more extreme case than SNe 1994W and 1995G, with 20–50 times more mass ejected in its precursor event, and a more energetic SN explosion. Consequently, diffusion through the opaque CSM shell made a more important contribution to the total luminosity as SN 2006gy remained fully optically thick (i.e., R_{BB} was equal to the true shock radius) out to much larger distances. This is why SN 2006gy had a smaller $H\alpha$ equivalent width than the other two events (see Figures 5 and 12). Qualitatively, though, all three SNe showed similar absorption features in their spectra (Fig. 5). As discussed above, some other SNe IIn like SN 1998S and SN 2005gl passed through qualitatively similar phases that, however, lasted only a short time, implying that they are very slimmed-down versions of similar phenomena.

We have not invoked a high degree of clumping in the CSM of SN 2006gy, because clumping allows the blast wave to propagate relatively unimpeded through the lower-density interclump regions (i.e., the shock remains fast), it facilitates the escape of copious X-rays,

and it allows an observer to see radiation from the underlying SN photosphere. These traits are not observed in SN 2006gy. This is a key difference between SN 2006gy and models for less luminous (but X-ray bright) SNe IIn like SN 1988Z and SN 2005ip, where a clumped CSM was invoked for these reasons (Chugai & Danziger 1994; Smith et al. 2009a). This is also a difference between our model for SN 2006gy and that of Agnoletto et al. (2009), who assumed strong clumping.

4.4. Evaluation of the PISN Hypothesis

In Paper I we noted that the extraordinary peak luminosity of SN 2006gy requires exceptional physical conditions unlike those of previous SNe. If radioactivity is the luminosity source, then an unusually large mass of ^{56}Ni near $10 M_{\odot}$ would be required, which in turn would necessitate a PISN (e.g., Barkat et al. 1967; Rakavy & Shaviv 1967; Bond et al. 1984; Heger & Woosley 2002). If, on the other hand, CSM interaction were the engine, then a surprisingly large mass of CSM would be needed, comparable to the 10–20 M_{\odot} of H-rich material ejected in observed giant LBV eruptions such as the 1843 event of η Carinae (Paper I; Smith et al. 2003) or some event like theoretical pulsational pair-instability eruptions (Woosley et al. 2007). In Paper I we were unable to choose between those two possibilities because both presented challenges, as noted in the introduction.

After considering the spectral evolution of SN 2006gy in detail, we find that most of its physical and morphological properties can be interpreted in the context a two-component CSM-interaction model. The apparent contradictions of a simple CSM-interaction model that were noted in Paper I can be reconciled with observations by pushing the physical conditions — in particular the optical depth and CSM mass — to extremes. High optical depths lead to a situation where the luminosity of SN 2006gy is powered by a two-component engine: radiative diffusion from $\sim 10^{51} \text{ erg}$ of shock-deposited thermal energy dominates at early times, while an increasing fraction at later times is supplied by the normal scenario of direct radiative post-shock cooling. This two-component CSM interaction engine seems to alleviate the need for an internal energy source such as radioactive decay from $10 M_{\odot}$ of ^{56}Ni because it reconciles the high CSM interaction luminosity with the seemingly paradoxical weakness of CSM interaction diagnostics like $H\alpha$ and X-ray emission.

Two final points are worth emphasizing, however. First, the extremely dense and massive CSM required for SN 2006gy does seem to be quite well explained by the predictions of Woosley et al. (2007) for a pulsational pair-instability ejection. This event has the same underlying instability, but results in a nonterminal precursor explosion because the energy generation is insufficient to completely unbind the star. It is expected to occur for stars with initial masses in the range 95–135 M_{\odot} , just shy of the extremely high masses required for a true PISN (see Heger et al. 2003). Second, the late-time (day 200–240) luminosity of SN 2006gy is still a problem, and it remains difficult to decisively rule out some contribution from radioactive decay. The late-time luminosity is sustained even though diagnostics of the optically thin CSM interaction ($H\alpha$, Fe II, Ca II) plummet. This luminosity at 200–240 days cannot be mostly due to a light

echo (which *does* dominate 1 yr later; Smith et al. 2008b; Miller et al. 2009b) because the optical spectrum is different than at peak, and because of the strength of broad absorption features in the spectrum (see §3.7).

4.5. Implications for SN 2005ap and SN 2008es

The high peak luminosity of SN 2006gy has been exceeded by two recent SNe, SN 2005ap (Quimby et al. 2007) and SN 2008es (Miller et al. 2009a; Gezari et al. 2009). The interesting twist, though, is that neither of these had a Type II_n spectrum, unlike all the luminous runners-up. It is therefore not obvious that their luminosity is generated by CSM interaction.

In this paper we have found that SN 2006gy exploded in a dense two-component CSM, with a massive opaque inner shell within a radius of $(2-4) \times 10^{15}$ cm, plus a more extended circumstellar envelope with an outer boundary of roughly 10^{16} cm. We have concluded that it was largely the diffusion of radiation from interaction with the inner opaque shell that powered its rise to peak luminosity, as proposed by Smith & McCray (2007), while the continued CSM interaction with the more extended shell powered some of the continuum luminosity at late times and determined the H α luminosity, soft X-ray luminosity, and unusual absorption and emission-line profiles. Photoionization of this outer shell produced the narrow emission-line components in the spectrum. If this outer shell had not been present, however, SN 2006gy would not have had a Type II_n spectrum.

The outer radius of the outer shell of SN 2006gy at $\sim 10^{16}$ cm was determined primarily by the maximum velocity of the precursor mass ejection and the fact that it occurred 8 yr before explosion. If that ejection episode had less mass and energy, or if it had occurred a shorter time before the final SN, the resulting CSM envelope may have been less massive and/or more compact. By varying the physical properties of the precursor ejection, we can understand the variety of observed properties in the most luminous SNe. A lower CSM mass would have resulted in faster final expansion speeds due to conservation of momentum. The lower CSM mass would also cause a faster diffusion time — and hence, more rapid rise and decay times — for interaction with the opaque shell. Without the more extended shell, there would have been no ongoing optically thin CSM interaction to drive the Type II_n spectrum. Thus, with a modified set of pre-SN conditions, one can see how a similar type of CSM interaction could power both SN 2005ap and SN 2008es. We therefore consider it unlikely that these events were true PISNe. Their properties, however, do seem consistent with pre-SN shell ejections triggered by a pulsational pair instability, or perhaps some other as-yet unidentified explosive instability.

4.6. The Precursor Event: LBV Eruption or the Pulsational Pair Instability?

In Paper I and in this work, we have noted a number of similarities between the inferred physical properties of the mass ejection that occurred 8 yr before SN 2006gy and the observed properties of giant LBV eruptions like the 1843 event of η Carinae. The most important of these are the total ejected mass of 10–20 M_{\odot} (Smith et al. 2003), launched at speeds of 100–600 km s⁻¹ with a

Hubble-like velocity law indicating a brief event (Smith 2006a), and the H-rich composition. We have also noted that these properties, and the fact that the outburst occurred within a decade of the SN, seem equally consistent with a precursor event caused by the pulsational pair instability (Woosley et al. 2007).

We wish to emphasize that *these two scenarios are not necessarily mutually exclusive*. One is observational (the comparison to observed LBV eruptions like η Car), and the other is a theoretical idea (the pulsational pair instability). We cannot rule out the possibility that they are, in fact, the same phenomenon, since we still do not know what triggered the 1843 outburst of η Car. After all, most of the observed properties of η Car’s giant eruption are consistent with expectations of the pulsational pair instability, except that η Car has not yet met its final demise even though it suffered similar previous outbursts ~ 1000 yr ago. Judging by the additional massive ~ 10 – $20 M_{\odot}$ dust shell required for the late-time IR light echo of SN 2006gy (Smith et al. 2008b; Miller et al. 2009b), it also appears to have suffered a previous shell ejection event ~ 1500 yr ago. Heger & Woosley (2002) have noted that in some cases, the time between successive pair pulsations can reach as much as ~ 1000 yr. Furthermore, recent observations of η Car have shown that it even had an explosive component to the event that created a fast (~ 5000 km s⁻¹) blast wave out ahead of the most massive material (Smith 2008).

4.7. Implications for Massive-Star Evolution: The Role of LBVs?

Regardless of whether SN 2006gy was a PISN or instead a sequence of pre-SN shell ejections caused by pair pulsations or some other mechanism, we argued in Paper I that the extreme energy and mass budgets make it difficult to avoid the requirement that SN 2006gy marked the death of a very massive star. The work described here reinforces this view: we find that the amount of CSM required is $\sim 20 M_{\odot}$, and that the mass of SN ejecta must be comparable in order to yield the final efficiency of about 50% in converting kinetic energy to light. Furthermore, our previous study of the late-time IR emission (Smith et al. 2008b) suggested a dust shell with a total gas mass of at least 10 M_{\odot} ejected 1000–2000 yr ago. This mass budget requires that within $\sim 10^3$ yr of its final explosion, the progenitor star still retained no less than 40–50 M_{\odot} .

A key point to recall is that SN 2006gy occurred in a galaxy of roughly solar metallicity, so the progenitor star would have shed significant mass during its lifetime and its *initial* mass was probably well above 100 M_{\odot} . This is consistent with models for SN 2006gy as a pulsational pair event (Woosley et al. 2007), which involved a star with an initial mass of 110 M_{\odot} . (Similar requirements appear to be necessary for SN 2006tf, but the mass budgets are more relaxed for SNe 2005ap and 2008es.)

Therefore, it seems impossible that SN 2006gy was a thermonuclear (Type Ia) SN that exploded in a dense H-rich CSM to produce a Type II_n spectrum, as had been suggested for SNe 2002ic and 2005gj (Hamuy et al. 2003; Chugai & Yungelson 2004; Aldering et al. 2006; Prieto et al. 2007), and possibly also SNe 1997cy and 1999E (Germany et al. 2000; Turatto et al. 2003; Rigon et al. 2003). These had been the most luminous SNe known

until SN 2006gy was discovered. We have noted that in several *observed* respects, SN 2006gy can be regarded as a more extreme case of this class of objects. It therefore seems possible that not all of them are SNe Ia in dense CSM environments either, supporting the view of Benetti et al. (2006). Trundle et al. (2008) have also expressed doubt that SN 2005gj was a Type Ia event because of similarities between its pre-shock CSM and the winds of LBV stars.

If SN 2006gy really was the death of a very massive star, it challenges the standard paradigm that all massive stars at near-solar metallicity should shed their H envelopes and explode as Wolf-Rayet (WR) stars (Conti 1976; Chiosi & Maeder 1986), yielding SNe of Type Ib or Ic and possibly gamma-ray bursts (e.g., Langer et al. 1994; Maeder & Meynet 1994; Heger et al. 2003; Woosley & Heger 2006). Instead, it requires that some extremely massive stars are able to retain substantial H envelopes up until or immediately before the time of core collapse.

This brings to mind the recent recognition that steady line-driven mass-loss rates of O-type stars and WR stars are lower than those included in most models. The winds are clumped, which lowers the mass-loss rate one derives from observations (see Bouret et al. 2005; Fullerton et al. 2006). Lower mass-loss rates for the 3–5 Myr on the main sequence could substantially increase a star’s final mass. Smith & Owocki (2006) pointed out that LBV eruptions may help make up some of the deficit, but if insufficient, the star can explode as an LBV with part of its H envelope still intact.

We have argued here and elsewhere (Smith et al. 2007, 2008a, 2008b; Smith 2006b) that the extreme progenitor mass-loss rates required to produce the dense CSM around luminous SNe IIn may suggest a link to LBV-like instability in the progenitor stars. LBVs in eruption are the *only* stars that are observed to have mass-loss rates of the correct order to explain more luminous SNe IIn. Furthermore, there is empirical evidence that the mass shedding by luminous SN IIn progenitors is not due to steady winds, but is instead from episodic bursts of mass loss like LBV eruptions. Outer shells around at least some SNe, such as the dusty IR echo shell around SN 2006gy (Smith et al. 2008b), imply that these eruption episodes are recurrent on a timescale of $\sim 10^3$ yr, like LBVs. (We have also noted, however, that some of the less luminous SNe IIn, such as SN 2005ip, can potentially be explained with the most extreme cases of RSG mass loss, so not *all* SNe IIn necessarily come from LBVs; see Smith et al. 2009a, 2009c.)

The possibility of a LBV/SN IIn connection, inferred indirectly from pre-SN CSM properties, has been confirmed by the only case so far where a SN IIn progenitor star has been identified directly in pre-explosion images. In SN 2005gl it was found that the progenitor did in fact resemble a very luminous LBV-like star with high luminosity (Gal-Yam et al. 2007, Gal-Yam & Leonard 2009). Gal-Yam & Leonard found that the progenitor had a temperature consistent with LBVs (i.e., a blue to yellow supergiant, not a RSG) and a very high luminosity of $\sim 10^6 L_{\odot}$. They also demonstrated that this star vanished after SN 2005gl faded. If the progenitor luminosity is the true luminosity of the quiescent star (and not, for example, the enhanced luminosity caught

during a giant eruption precursor event), then a very massive progenitor with initial mass above $\sim 50 M_{\odot}$ is required. To explain the observed level of CSM interaction in SN 2005gl, Gal-Yam & Leonard (2009) find that the precursor shell ejection event had a mass-loss rate of $\sim 0.03 M_{\odot} \text{ yr}^{-1}$, similar to the 1600 AD giant eruption of the famous LBV star P Cygni (Smith & Hartigan 2006). The fact that SN 2005gl itself was not a particularly high-luminosity event compared to other SNe IIn underscores the truly astonishing set of conditions that led to SN 2006gy. The progenitor of SN 2006gy must have been an extreme case of an already extraordinary class of stars.

There are several other circumstantial indications that LBVs may be related to SNe as well, mainly from inferred properties of the H-rich pre-shock CSM (Salamanca et al. 2002; Kotak & Vink 2006; Smith 2006b, 2007; Smith et al. 2007, 2008a, 2008b; Trundle et al. 2008). One argument made by these authors is that the speed and possible variability of the pre-shock CSM is close to the outflow speeds of a few hundred km s^{-1} observed in LBVs, while being much faster than RSG winds and slower than WR winds. This is true for SN 2005gl as well (see the Appendix). Wind speeds alone are not conclusive, since radiation from the SN itself may accelerate pre-shock CSM to these speeds. This could, in principle, cause the two-component absorption features in SN 2005gj that Trundle et al. (2008) showed to be very similar to $H\alpha$ profiles in the LBV star AG Carinae. While not conclusive on their own, the pre-shock speeds are nevertheless consistent with the LBV interpretation. They can be taken together with the large CSM masses needed to power the luminosity (discussed in this work) and the similarity between LBV nebulae and the pre-SN nebula around SN 1987A (Smith 2007) to support the view that in some cases, LBV episodes may indeed precede SNe.

If other SNe IIn are also very massive stars that retain their H envelopes until just before their death, it suggests a picture where these stars enter a phase of instability shortly before explosion that triggers the ejection of much or all of their remaining H envelopes. The underlying SN explosion, which, hypothetically, may otherwise have been a Type Ia, Ib/c, IIf, II-P, or II-L event, expands into that recently ejected massive H envelope to produce a SN IIn. (In this regard, it may be more appropriate to consider the Type IIn classification as a phenomenon rather than a class of explosions.) One might expect a very massive star nearing core collapse to be unstable if it has retained part of its H envelope, because its outer H envelope would be dangerously close to, or may substantially exceed, the classical Eddington limit. The attempt to understand this phenomenon is likely to benefit from continued study of the physics of giant LBV eruptions and theoretical investigations of super-Eddington winds (e.g., Owocki et al. 2004; van Marle et al. 2009a), even though it is not yet clear if the two phenomena have the same underlying trigger. Such pre-SN instability might be exacerbated by additional luminosity from final burning stages. A star could therefore be subject to periodic and sudden bursts of mass loss as it tries to shed its massive H envelope. These clues suggest that the final years of very massive stars include sporadic events that essentially *determine* the end fate of the star. Significant revision is therefore needed to correctly model

and predict the fates of the most massive stars beyond our speculation noted here, including dynamical events like LBV eruptions, pulsational pair ejections, or other instabilities associated with late phases.

N.S. acknowledges relevant discussions with S. Woosley and A. Heger. We thank the following observers who assisted with runs at Lick Observatory: M. Ganeshalingam, M. Moore, D. Pooley, S. Rodney, T.N. Steele, and D.S. Wong. Some of the data presented herein were obtained at the W. M. Keck Observatory, which is operated as a scientific partnership among the California Institute of Technology, the University of California, and the National Aeronautics and Space Administration (NASA); the observatory was made possible by the gen-

erous financial support of the W. M. Keck Foundation. We wish to extend special thanks to those of Hawaiian ancestry on whose sacred mountain we are privileged to be guests. We are grateful to the staffs at the Lick and Keck Observatories for their dedicated services. KAIT and its ongoing operation were made possible by donations from Sun Microsystems, Inc., the Hewlett-Packard Company, AutoScope Corporation, Lick Observatory, the National Science Foundation (NSF), the University of California, the Sylvia & Jim Katzman Foundation, and the TABASGO Foundation. This research was supported by NSF grant AST-0607485, the TABASGO Foundation, and NASA/*HST* grant GO-10877 from the Space Telescope Science Institute (STScI), which is operated by AURA, Inc., under NASA contract NAS 5-26555. N.S. was partially supported by grants GO-10241 and GO-10475 from STScI.

Facilities: Keck I (LRIS, LRISP), Keck II (DEIMOS), Lick 3 m (Kast).

REFERENCES

- Agnoletto, I., et al. 2009, *ApJ*, 691, 1348
 Aldering, G., et al. 2006, *ApJ*, 650, 510
 Aretxaga, I., et al. 1999, *MNRAS*, 309, 343
 Barkat, Z., Rakavy, G., & Sack, N. 1967, *PRL*, 18, 379
 Benetti, S., Cappellaro, E., Turatto, M., Taubenberger, S., Harutyunyan, A., & Valenti, S. 2006, *ApJ*, 654, L129
 Bessell, M. S. 1999, *PASP*, 111, 1426
 Bietenholz, M., & Bartel, N. 2007, *ATel*, 1254, 1
 Branch, D., Jeffery, D. J., Blaylock, M., & Hatano, K. 2000, *PASP*, 112, 217
 Bregman, J. N., & Pildis, R. A. 1992, *ApJ*, 398, L107
 Bond, J. R., Arnett, W. D., & Carr, B. J. 1984, *ApJ*, 280, 825
 Bouret, J. C., Lanz, T., & Hillier, D. J. 2005, *A&A*, 438, 301
 Canizares, C. R., Kriss, G. A., & Feigelson, E. D. 1982, *ApJ*, 253, L17
 Cardelli, J. A., Clayton, G. C., & Mathis, J. S. 1989, *ApJ*, 345, 245
 Chevalier, R. A. 1977, *ARAA*, 15, 175
 Chevalier, R. A. 2003, *LNP*, 598, 171
 Chiosi, C., & Maeder, A. 1986, *ARAA*, 24, 329
 Chugai, N. N. 1990, *Sov. Astron. Lett.*, 16, 457
 Chugai, N. N. 2001, *MNRAS*, 326, 1448
 Chugai, N. N., & Chevalier, R. A. 2006, *ApJ*, 657, 378
 Chugai, N. N., & Chevalier, R. A., & Lundqvist, P. 2006, *MNRAS*, 355, 627
 Chugai, N. N., & Danziger, I. J. 1994, *MNRAS*, 268, 173
 Chugai, N. N., & Danziger, I. J. 2003, *Ast. Letters*, 29, 649
 Chugai, N. N., & Yungelson, L. R. 2004, *Ast. Letters*, 30, 83
 Chugai, N. N., Blinnikov, S. I., Fassia, A., Lundqvist, P., Meikle, W. P. S., & Sorokin, E. I. 2002, *MNRAS*, 330, 473
 Chugai, N. N., Blinnikov, S. I., Cumming, R. J., Lundqvist, P., Bragaglia, A., Filippenko, A. V., Leonard, D. C., Matheson, T., & Sollerman, J. 2004, *MNRAS*, 352, 1213
 Conti, P. S. 1976, *Mem. Soc. R. Sci. Liege*, 9, 193
 Deng, J., Kawabata, K. S., Ohyama, Y., Nomoto, K., Mazzali, P. A., Wang, L., Jeffery, D. J., Iye, M., Tomita, H., & Yoshii, Y. 2004, *ApJ*, 605, L37
 Dessart, L., & Hillier, D. J. 2008, *MNRAS*, 383, 57
 Dessart, L., Hillier, D. J., Gezari, S., Basa, S., & Matheson, T. 2009, *MNRAS*, 394, 21
 Dopita, M. A., Evans, R., Cohen, M., & Schwarz, R. D. 1984, *ApJ*, 287, L69
 Faber, S. M., et al. 2003, *Proc. SPIE*, 4841, 1657
 Falk, S., & Arnett, W. D. 1977, *ApJS*, 33, 515
 Fassia, A., et al. 2000, *MNRAS*, 318, 1093
 Fassia, A., et al. 2001, *MNRAS*, 325, 907
 Filippenko, A. V. 1982, *PASP*, 94, 715
 Filippenko, A. V. 1997, *ARAA*, 35, 309
 Foley, R. J., et al. 2003, *PASP*, 115, 1220
 Fullerton, A. W., Massa, D. L., & Prinja, R. K. 2006, *ApJ*, 637, 1025
 Gal-Yam, A., et al. 2007, *ApJ*, 656, 372
 Gal-Yam, A., & Leonard, D. C. 2009, *Nature*, 458, 865
 Germany, L. M., Reiss, D. J., Sadler, E. M., Schmidt, B. P., & Stubbs, C. W. 2000, *ApJ*, 533, 320.
 Gezari, S., et al. 2009, *ApJ*, 690, 1313
 Grazberg, E., & Nadëzhin, D. 1986, *Sov. Ast. Lett.*, 12, 68
 Grazberg, E., & Nadëzhin, D. 1987, *Sov. Astron.*, 31, 629
 Hamuy, M., et al. 2003, *Nature*, 424, 651
 Heger, A., & Woosley, S. E. 2002, *ApJ*, 567, 532
 Heger, A., Fryer, C. L., Woosley, S. E., Langer, N., & Hartmann, D. H. 2003, *ApJ*, 591, 288
 Hoffman, J. L., Leonard, D. C., Chornock, R., Filippenko, A. V., Barth, A. J., & Matheson, T. 2008, *ApJ*, 688, 1186
 Kawabata, K. S., Tanaka, M., Maeda, K., Hattori, T., Nomoto, K., Tominaga, N., & Yamanaka, M. 2009, *ApJ*, 697, 747
 Kotak, R., & Vink, J. S. 2006, *A&A*, 460, L5
 Kotak, R., Meikle, W. P. S., Adamson, A., & Leggett, S. K. 2004, *MNRAS*, 354, L13
 Langer, N., Hamann, W. R., Lennon, M., Najarro, F., Pauldrach, A. W. A., & Puls, J., 1994, *A&A*, 290, 819
 Leibundgut, B., et al. 1991, *ApJ*, 372
 Lentz, E. J., et al. 2001, *ApJ*, 547, 406
 Leonard, D. C., et al. 2000, *ApJ*, 536, 239
 Leonard, D. C., et al. 2002, *PASP*, 114, 35
 Matheson, T., Filippenko, A. V., Ho, L. C., Barth, A. J., & Leonard, D. C. 2000, *AJ*, 120, 1499
 Miller, J. S., & Stone, R. P. S. 1993, *Lick Obs. Tech. Rep. 66* (Santa Cruz: Lick Obs.)
 Miller, A. A., et al. 2009a, *ApJ*, 690, 1303
 Miller, A. A., et al. 2009b, *AJ*, submitted (arXiv:0906.2201)
 Nomoto, K., et al. 2007, in *SN 1987A: 20 Years After: Supernovae and Gamma Ray Bursters*, ed. S. Immler, K. Weiler, & R. McCray (New York: AIP), 412
 Ofek, E. O., et al. 2007, *ApJ*, 659, L13
 Oke, J. B., et al. 1995, *PASP*, 107, 375
 Owocki, S. P., Gayley, K. G., & Shaviv, N. J. 2004, *ApJ*, 616, 525
 Pastorello, A., Turatto, M., Benetti, S., Cappellaro, E., Danziger, I. J., Mazzali, P. A., Patat, F., Filippenko, A. V., Schlegel, D. J., & Matheson, T. 2002, *MNRAS*, 333, 27
 Pooley, D., et al. 2002, *ApJ*, 572, 932
 Portegies Zwart, S. F., & van den Heuvel, E.P.J. 2007, *Nature*, 450, 388
 Prieto, J., et al. 2007, arXiv:0706.4088
 Quimby, R., Aldering, G., Wheeler, J. C., Höflich, P., Akerlof, C. W., & Rykoff E. S. 2007, *ApJ*, 668, L99
 Rakavy, G., & Shaviv, G. 1967, *ApJ*, 148, 803
 Rigon, L., et al. 2003, *MNRAS*, 340, 191
 Ryder, S. D., et al. 1992, *IAUC*, 5615, 1
 Salamanca, I., Cid Fernandes, R., Tenorio-Tagle, G., Telles, E., Terlevich, R. J., & Munoz-Tunon, C. 1998, *MNRAS*, 300, L17
 Salamanca, I., Terlevich, R. J., & Tenorio-Tagle, G. 2002, *MNRAS*, 330, 844
 Scannapieco, E., Madau, P., Woosley, S. E., Heger, A., & Ferrara, A. 2005, *ApJ*, 633, 1031
 Schlegel, E. M. 1990, *MNRAS*, 244, 269
 Schlegel, E. M., & Petre, R. 2006, *ApJ*, 646, 378
 Smith, N. 2006a, *ApJ*, 644, 1151
 Smith, N. 2006b, astro-ph/0607457
 Smith, N. 2007, *AJ*, 133, 1034
 Smith, N. 2008, *Nature*, 455, 201
 Smith, N., Chornock, R., Li, W., Ganeshalingam, M., Silverman, J. M., Foley, R. J., Filippenko, A. V., & Barth, A. J. 2008a, *ApJ*, 686, 467
 Smith, N., & Hartigan, P. 2006, *ApJ*, 638, 1045
 Smith, N., Hinkle, K. H., & Ryde, N. 2009c, *AJ*, 137, 3558
 Smith, N., Li, W., Foley, R. J., Wheeler, J. C., Pooley, D., Chornock, R., Filippenko, A. V., Silverman, J. M., Quimby, R., Bloom, J., & Hansen, C. 2007, *ApJ*, 666, 1116
 Smith, N., & McCray, R. 2007, *ApJ*, 671, L17
 Smith, N., & Owocki, S. P. 2006, *ApJ*, 645, L45
 Smith, N., et al. 2003, *AJ*, 125, 1458
 Smith, N., et al. 2008b, *ApJ*, 686, 485

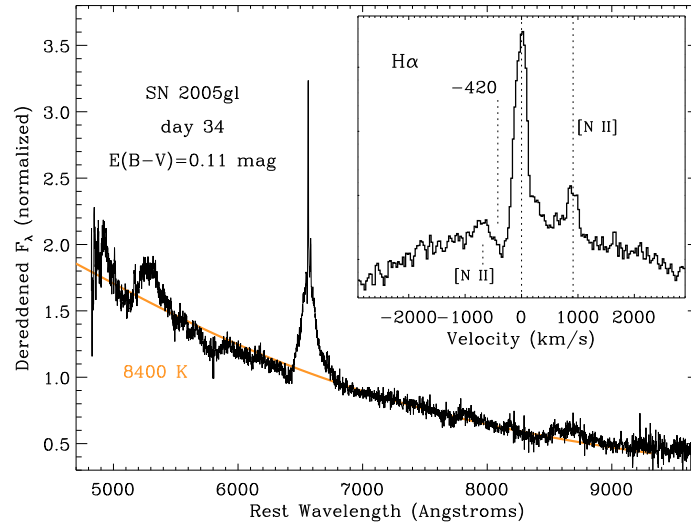


FIG. 26.— The day 34 spectrum of SN 2005gl obtained with DEIMOS, dereddened by $E(B - V) = 0.11$ mag. An 8500 K blackbody is shown for comparison (gray; orange in the online edition). The inset shows the narrow $H\alpha$ profile. The dashed vertical lines indicate the pre-shock speed of 420 km s^{-1} estimated by Gal-Yam & Leonard (2009), as well as the expected location of [N II] lines.

Smith, N., et al. 2009a, ApJ, 695, 1334
 Smith, N., et al. 2009b, ApJ, 697, L49
 Sollerman, J., Cumming, R. J., & Lundqvist, P. 1998, ApJ, 493, 933
 Trundle, C., Kotak, R., Vink, J. S., & Meikle, W. P. S. 2008, A&A, 483, L47
 Turatto, M., et al. 2000, ApJ, 534, L57
 Turatto, M., et al. 1993, MNRAS, 262, 128
 Van Dyk, S. D., Weiler, K. W., Sramek, R. A., & Panagia, N. 1993, ApJ, 419, L69
 van Marle, A. J., Owocki, S. P., & Shaviv, N. J. 2009a, MNRAS, 394, 595

van Marle, A. J., Smith, N., & Owocki, S. P. 2009b, MNRAS, submitted
 Wang, L., Baade, D., Höflich, P., Wheeler, J. C., Kawabata, K., & Nomoto, K. 2004, ApJ, 604, L53
 Williams, C. L., Panagia, N., Van Dyk, S. D., Lacey, C. K., Weiler, K. W., & Sramek, R. A. 2002, ApJ, 581, 396
 Wood-Vasey, W. M., Wang, L., & Aldering, G. 2004, ApJ, 616, 339
 Woosley, S. E., & Heger, A. 2006, ApJ, 637, 914
 Woosley, S. E., Blinnikov, S., & Heger, A. 2007, Nature, 450, 390

APPENDIX

SN 2005gl is a special case among SNe IIn because it is the only one, so far, for which a progenitor star has been identified in pre-explosion images. Gal-Yam et al. (2007) and Gal-Yam & Leonard (2009) have already analyzed the spectral evolution of this SN, including spectra obtained on days 8, 58, and 87 after discovery. In this Appendix, we present an additional unpublished spectrum of SN 2005gl because our higher-resolution data provide new information on the progenitor’s wind speed, and are therefore pertinent to our study of SN 2006gy through the LBV/SN IIn connection.

We observed SN 2005gl using DEIMOS/Keck II on 2005 November 8, roughly 34 days after discovery. This is between the first and second epochs of spectra published by Gal-Yam et al. (2007), when the SN transitioned from one where Type IIn features dominated the spectrum, to one that looked more like a Type II-P. Indeed, if we adopt a reddening correction of $E(B - V) = 0.11$ mag (Gal-Yam et al. 2007), we find a characteristic continuum temperature of ~ 8500 K (Figure 26) that is intermediate between the value of 13,000 K on day 8 and a lower temperature around 6000–6500 K on day 58. Except for the narrow component, the spectrum is consistent with those of SNe II-P at comparable epochs, with a half-width at zero intensity (HWZI) for the red wing of the broad $H\alpha$ component of $\sim 10^4 \text{ km s}^{-1}$.

Of particular interest is that our spectrum has higher dispersion ($R = \lambda/\Delta\lambda \approx 3000$) than previous data, resolving the narrow emission component and revealing the presence of narrow P Cygni absorption. Gal-Yam & Leonard (2009) used the HWZI of the narrow $H\alpha$ profile, which was marginally unresolved in their spectra, to estimate a pre-shock outflow speed of $\sim 420 \text{ km s}^{-1}$ (shown by the dashed line in Figure 26). Our spectrum, where the line width is fully resolved, yields a slightly faster FWZI on the red side of roughly 600 km s^{-1} , although the line exhibits some complex structure. Similarly, our spectrum shows significant blueshifted P Cygni absorption out to roughly -600 km s^{-1} as well (this is complicated by [N II] $\lambda 6548$ emission, but absorption is nevertheless present at these speeds). Although 600 km s^{-1} is faster than the 420 km s^{-1} estimated by Gal-Yam & Leonard (2009), it supports their claim that the speed is similar to ejecta of LBVs like η Car (Smith 2006). In this paper and Paper I, we have discussed the same type of evidence for comparable speeds in the pre-shock CSM of SN 2006gy and made similar connections to LBV-like stars. These connections are reinforced by the speeds observed in the CSM of SN 2005gl.